WRDC-TR-89-2120

AIRBORNE/SPACEBORNE PULSED POWER SOURCE

George Z. Hutcheson

Mission Research Corporation
1720 Randolph Road, SE
Albuquerque, NM 87106

August 1989

Final Report for Period August 1988 - April 1989

AERO PROPULSION AND POWER LABORATORY
WRIGHT RESEARCH AND DEVELOPMENT CENTER
AIR FORCE SYSTEMS COMMAND
WRIGHT-PATTERSON AIR FORCE BASE, OHIO 45433-6563

NOTICE

When Government drawings, specifications, or other data are used for any purpose other than in connection with a definitely Government-related procurement, the United States Government incurs no responsibility or any obligation whatsoever. The fact that the government may have formulated or in any way supplied the said drawings, specifications, or other data, is not to be regarded by implication, or otherwise in any manner construed, as licensing the holder, or any other person or corporation; or as conveying any rights or permission to manufacture, use, or sell any patented invention that may in any way be related thereto.

This report is releasable to the National Technical Information Service (NTIS). At NTIS, it will be available to the general public, including foreign nations.

This technical report has been reviewed and is approved for publication.

Lowell D. Massie

LOWELL D. MASSIE
Chief, Power Components Branch
Aerospace Power Division

FOR THE COMMANDER

WILLIAM U. BORGER
Chief, Aerospace Power Division
Aero Propulsion & Power Laboratory

If your address has changed, if you wish to be removed from our mailing list, or if the addressee is no longer employed by your organization please notify WRDC/POOC, WPAFB, OH 45433-6563 to help us maintain a current mailing list.

Copies of this report should not be returned unless return is required by security considerations, contractual obligations, or notice on a specific document.

REPORT DOCUMENTATION PAGE

1a. REPORT SECURITY CLASSIFICATION Unclassified	1b. RESTRICTIVE MARKINGS
2a. SECURITY CLASSIFICATION AUTHORITY	3. DISTRIBUTION/AVAILABILITY OF REPORT Approved for Public Release; Distribution is Unlimited.
2b. DECLASSIFICATION/DOWNGRADING SCHEDULE	
4. PERFORMING ORGANIZATION REPORT NUMBER(S) MRC/ABQ-R-1140	5. MONITORING ORGANIZATION REPORT NUMBER(S) WRDC-TR-89-2120
6a. NAME OF PERFORMING ORGANIZATION MISSION RESEARCH CORPORATION 6b. OFFICE SYMBOL (If applicable)	7a. NAME OF MONITORING ORGANIZATION Aero Propulsion and Power Lab (WRDC/POOC-4) Wright Research and Development Center
6c. ADDRESS (City, State, and ZIP Code) 1720 Randolph Road, SE Albuquerque, NM 87106	7b. ADDRESS (City, State, and ZIP Code) Wright-Patterson AFB, Oh 45433-6563
8a. NAME OF FUNDING/SPONSORING ORGANIZATION 8b. OFFICE SYMBOL (If applicable) AFWAL/POOC-4	9. PROCUREMENT INSTRUMENT IDENTIFICATION NUMBER F33615-88-C-2855
8c. ADDRESS (City, State, and ZIP Code)	10. SOURCE OF FUNDING NUMBERS PROGRAM ELEMENT NO: 65502F; PROJECT NO: 3005; TASK NO: 21; WORK UNIT ACCESSION NO: 19

11. TITLE (Include Security Classification)
AIRBORNE/SPACEBORNE PULSED POWER SOURCE

12. PERSONAL AUTHOR(S)
Hutcheson, George Z.

13a. TYPE OF REPORT	13b. TIME COVERED	14. DATE OF REPORT (Year, Month, Day)	15. PAGE COUNT
Final	FROM 88/08/15 TO 89/04/14	1989 August	

16. SUPPLEMENTARY NOTATION
This is a Small Business Innovation Research Program Report, Phase I

17. COSATI CODES			18. SUBJECT TERMS (Continue on reverse if necessary and identify by block number)
FIELD	GROUP	SUB-GROUP	Pulsed Power, Repetitively Pulsed, Compact, Lightweight

19. ABSTRACT (Continue on reverse if necessary and identify by block number)

Mission Research Corporation (MRC) has completed a design study for a compact lightweight pulsed power source for airborne and spaceborne applications. Two designs were developed during the contract period. Both designs were constrained to -500 kV output pulses, 10 Hz repetition rates, and 2 ft. diameters. The designs utilized high voltage pulse-forming networks (PFN) composed of liquid capacitors and air-core inductors. Dual resonance spiral strip transformers were incorporated into the designs for charging the PFNs from lower voltage capacitor banks. A mixture of water and ethylene glycol was used in the capacitor designs in order that the operating temperatures (-45° C to +110° C) of the designs could be extended beyond that of pure water.

A pulser built from the final design would be capable of nominally producing -500 kV, 100 ns, 10 Ω pulses (i.e., 3 kJ). Such a pulser would be 10.9 ft. long (without prime power, power conditioning, and load) and would weigh 1300 lbs (with power conditioning but without prime power and load). The design has

20. DISTRIBUTION/AVAILABILITY OF ABSTRACT	21. ABSTRACT SECURITY CLASSIFICATION
☐ UNCLASSIFIED/UNLIMITED ☒ SAME AS RPT ☐ DTIC USERS	Unclassified
22a. NAME OF RESPONSIBLE INDIVIDUAL Sandra Fries Carr	22b. TELEPHONE (Include Area Code) (513) 255-9190
	22c. OFFICE SYMBOL AFWAL/POOC-4

Continued from Block 19.

the unique advantage of being mechanically "tunable" to any desired pulse length (100 ns to 500 ns) or impedance (10 Ω to 50 Ω) as long as the output energy of the pulser is not changed from 3 kJ. However, the output energy may be extended to 4 kJ by adjusting the mixing ratio of water and ethylene glycol in the capacitors.

The first design, based upon the original goals of the study, would yield a pulser that would produce -500 kV, 200 ns, 100 Ω pulses. Due to a slow fall time, this pulser would generate 800 J pulses. The lower energy pulsed power source, however, could produce very fast rising pulses (about 1 ns) with little variations in the plateau of the voltage (9%).

ABSTRACT

Mission Research Corporation (MRC) has completed a design study for a compact lightweight pulsed power source for airborne and spaceborne applications. Two designs were developed during the contract period. Both designs were constrained to -500 kV output pulses, 10 Hz repetition rates, and 2 ft. diameters. The designs utilized high voltage pulse-forming networks (PFN) composed of liquid capacitors and air-core inductors. Dual resonance spiral strip transformers were incorporated into the designs for charging the PFNs from lower voltage capacitor banks. A mixture of water and ethylene glycol was used in the capacitor designs in order that the operating temperatures (-45° C to +110° C) of the designs could be extended beyond that of pure water.

A pulser built from the final design would be capable of nominally producing -500 kV, 100 ns, 10 Ω pulses (i.e., 3 kJ). Such a pulser would be 10.9 ft. long (without prime power, power conditioning, and load) and would weigh 1300 lbs (with power conditioning but without prime power and load). The design has the unique advantage of being mechanically "tunable" to any desired pulse length (100 ns to 500 ns) or impedance (10 Ω to 50 Ω) as long as the output energy of the pulser is not changed from 3 kJ. However, the output energy may be extended to 4 kJ by adjusting the mixing ratio of water and ethylene glycol in the capacitors.

The first design, based upon the original goals of the study, would yield a pulser that would produce -500 kV, 200 ns, 100 Ω pulses. Due to a slow fall time, this pulser would generate 800 J pulses. The lower energy pulsed power source, however, could produce very fast rising pulses (about 1 ns) with little variations in the plateau of the voltage (9%).

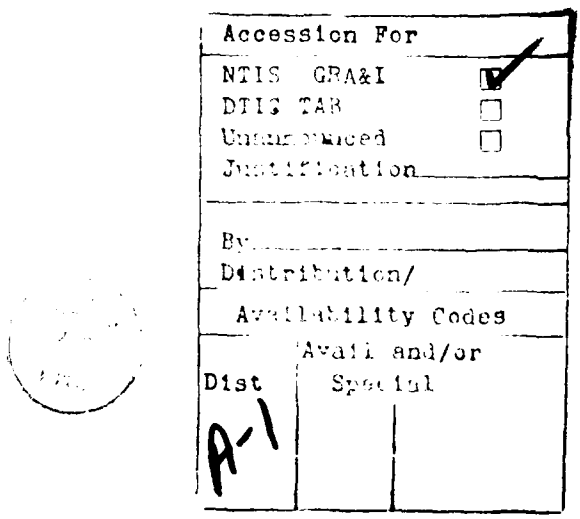

CONTENTS

FIGURES

FIGURES (CONTINUED)

FIGURES (CONCLUDED)

TABLES

1.0 INTRODUCTION

For many years now multi-gigawatt pulsed power systems have primarily been laboratory tools developed for a variety of applications. In the laboratory, there has been little or no effort in constructing lightweight compact pulsers. However, recent advances in directed energy technology and in high power devices will move these weapon and device concepts from the laboratory to the field. A major concern in fielding these new devices is the ability to build the electrical driving sources, the pulsed power, for these devices. The pulsed power sources must be capable of delivering the specified electrical requirements (e.g., voltage, impedance, pulse length, rise time, etc.) while not exceeding the mechanical and physical requirements (e.g., weight, volume, and simplicity) necessary for airborne and spaceborne systems.

This document describes a six month investigation conducted by Mission Research Corporation (MRC) for the Aero Propulsion Laboratory of the U.S. Air Force's Wright Aeronautical Laboratories to design a high voltage pulser capable of airborne and spaceborne operations. The original objectives of the study were to produce a design with blueprints for a pulsed power source with the following specifications:

a. 500 kilovolt output;

b. 200 nanosecond pulse length;

c. one nanosecond or less rise time;

d. 10 hertz repetition rate;

e. load impedance of 100 Ω in series with 25 nH; and

f. minimize weight and volume with 1,300,000 cm^3 and 600 pounds as design goals.

Additional specifications were imposed during the study period. These additional specifications were:

a. maximum 2 foot diameter cross-section;

b. voltage pulse flat top less than 15%;

c. maximize operating temperature;

d. maximize mission life;

e. minimize cost; and

f. maximize reliability and simplicity.

A design meeting these requirements was essentially completed and is detailed in Chapter 3. However, discussions with Air Force personnel altered the above design goals to higher energies (multi-kilojoules) and lower impedances (10 Ω) while maintaining all of the other requirements. Chapter 4 presents the results of the higher energy pulser design. Appendix A contains the component drawings for a 3 kJ pulser described in Chapter 4. Alternative pulse-forming networks (PFN) were examined and the results of this examination are presented in Chapter 2. In order to understand the evolution of the design, the remainder of this chapter describes the design approach presented in the Phase I proposal.

The original design as presented in the Phase I proposal (Ref. 1) utilized a lumped element Blumlein pulse-forming network (PFN) as shown in Figure 1. Each leg or side of the Blumlein was based on a Type B Guillemin network (Refs. 2, 3). Such Guillemin networks have been used since World War II in radar modulators to produce long pulse lengths in small volumes. The Blumlein was to be packaged in a low volume low weight geometry. Figure 2 is a sketch of the high voltage network. The shape may be described as a corrugated tri-plate geometry. The regions of minimum spacings between the center conductor and the corrugated sections formed the capacitors of the Blumlein; the regions of maximum spacing formed the inductors of the Blumlein. Water was added to the capacitor sections to increase the capacitance and reduce volume but an insulating gas was used for the inductor sections to reduce weight. The lengths and widths of the corrugated sections were to be adjusted to achieve the required values for the inductors and capacitors. The Blumlein was estimated to fit in a volume measuring 7 ft × 2 ft × 2.5 ft.

To achieve the fast rise times required, resistors were placed in parallel to the inductors nearest the load. These resistors dramatically reduced the rise time of the pulser as compared to the case where the resistors were not present without significantly reducing the energy delivered to the load. In a conventional lumped element pulse-forming network, the rise time is limited, approximately, by the sinusoidal rise associated with the inductor and capacitor combination of the last stage before the load. In the original design, the rise time was limited by the exponential folding time (i.e., L/R time) of the resistors and load in series with the stray inductances of the resistors, switch, and load. The use of the resistors along with appropriate timing of the closure of

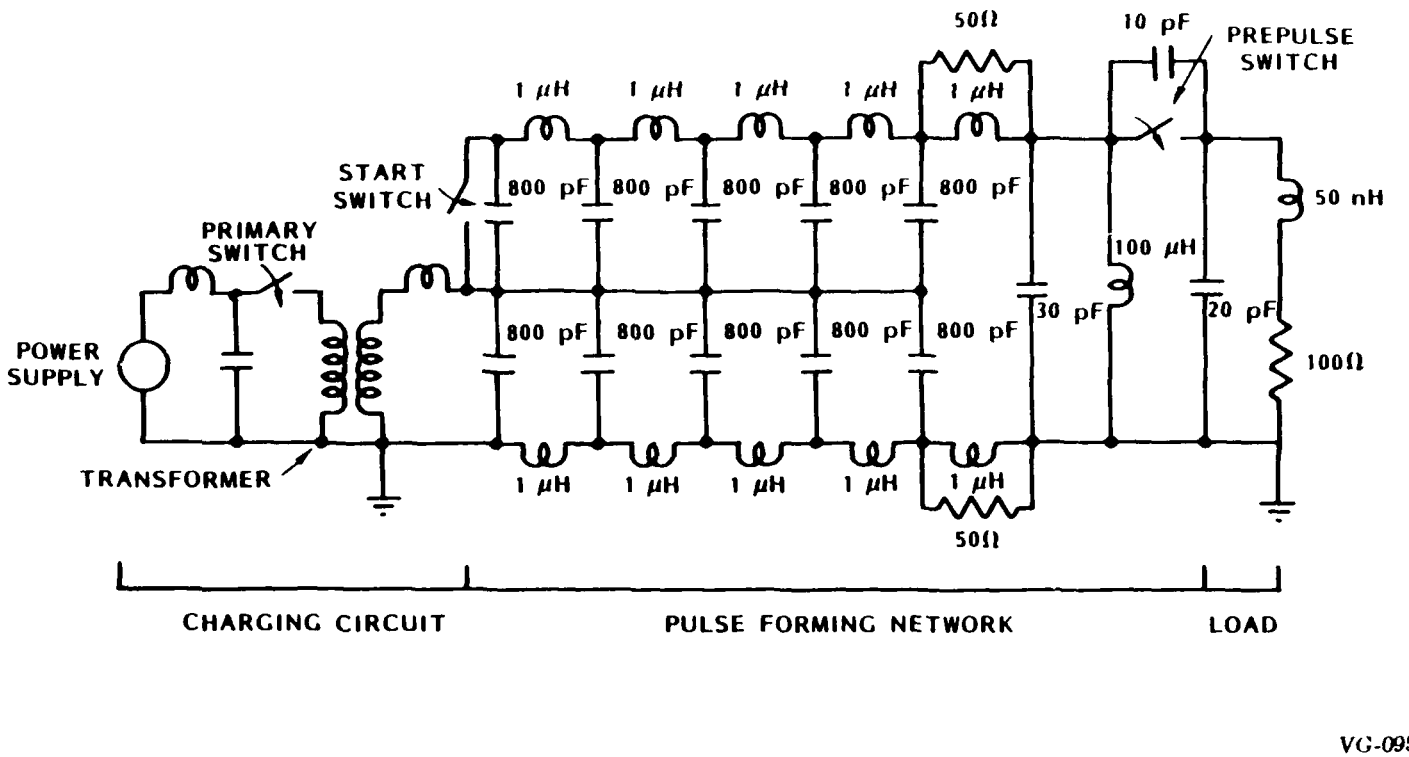

Figure 1. Circuit schematic of design in Phase I proposal.

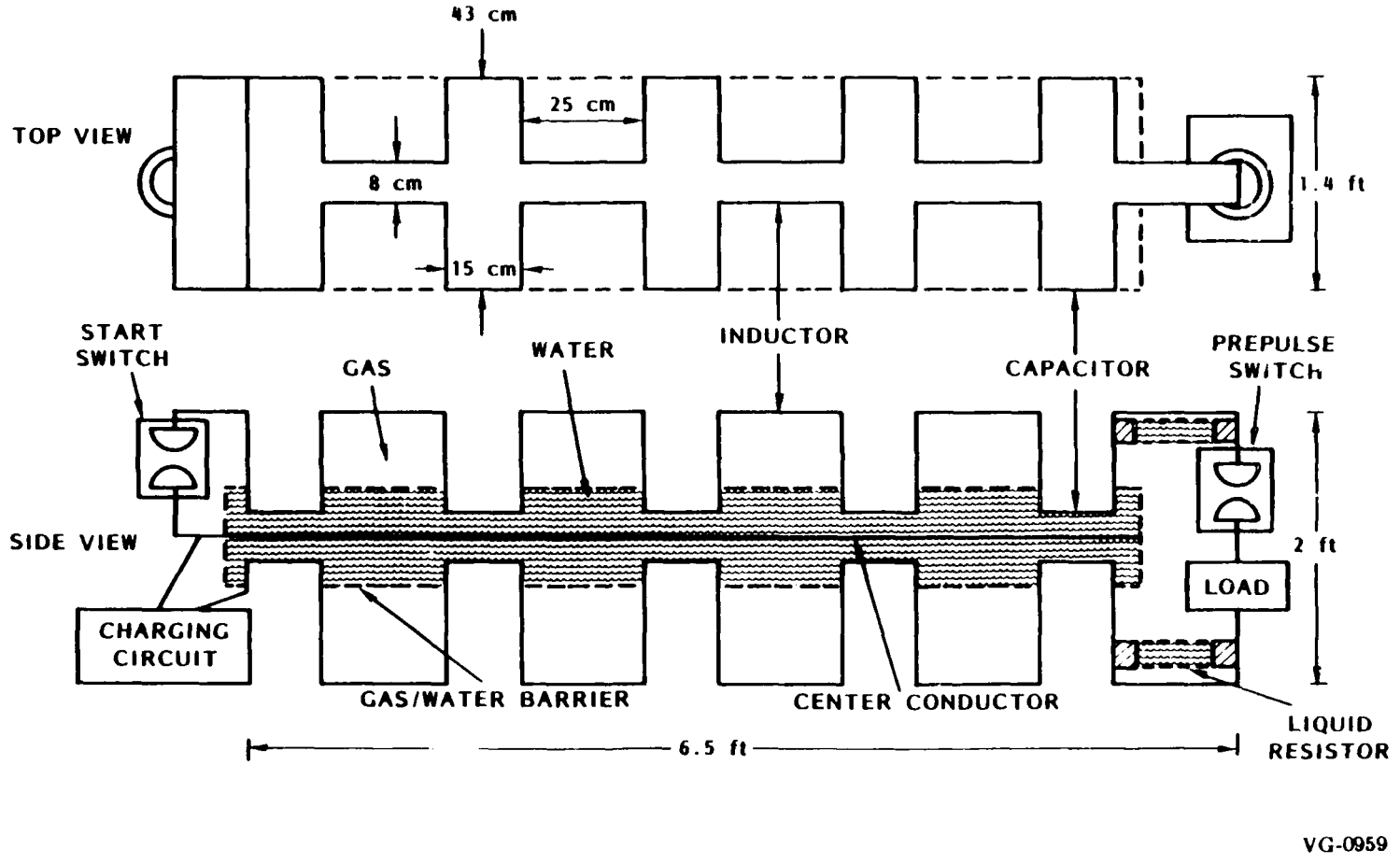

Figure 2. Physical layout of PFN in Phase I proposal.

the start and prepulse switches reduced the rise time by a factor of over 50 in circuit simulations. Figure 3 shows the output voltage pulse of the original design.

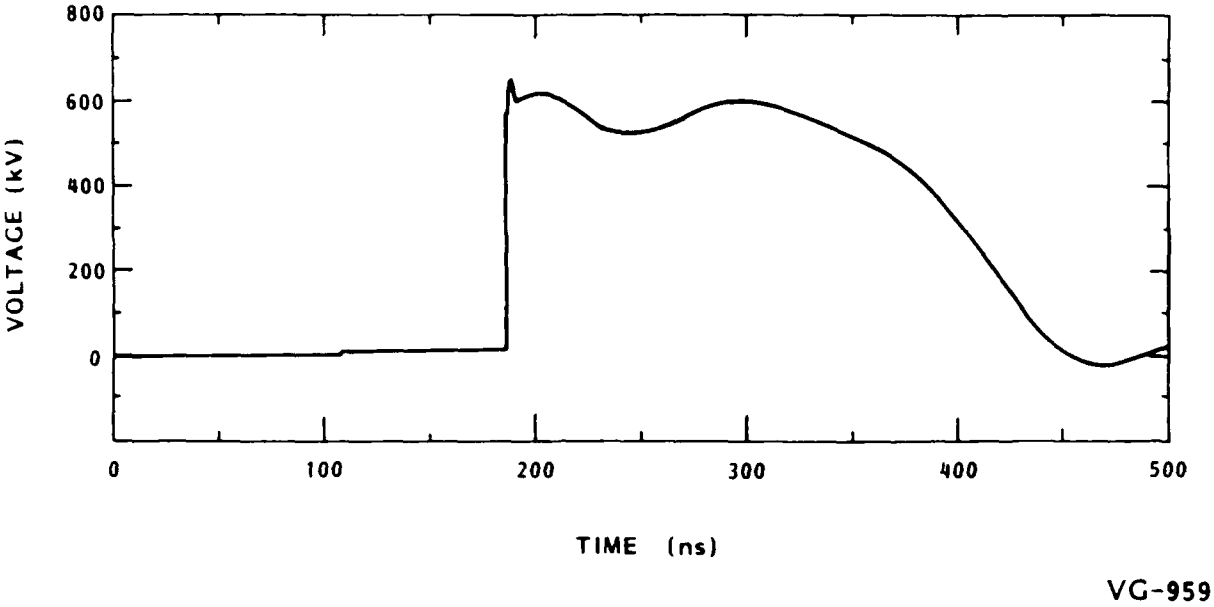

Figure 3. Output pulse of Phase I proposal pulser.

An air-core step-up transformer, operated in dual resonance, was to charge the Blumlein circuit. Such transformers can achieve 20 to 1 step-up ratios with better than 90% energy transfer from primary to secondary. Unlike Marx generators, transformers allow the initial energy storage capacitors (placed on the primary side of the transformer) to be completely operated at low voltages with a correspondingly reduced volume for voltage stand-off. Also, the initial energy storage capacitors can be switched into the PFN with only one switch as opposed to many switches required for Marx generators charging PFNs.

The original design was estimated to weigh less than 600 pounds and be contained in a volume of about 46 ft^3. Table 1 lists the weight, volume, and energy efficiencies of the original design.

During the course of the Phase I design study MRC conducted discussions with Air Force engineers and officers at the Aero Propulsion Laboratory and the Air Force Weapons Laboratory. Based upon these discussions, several of the specifications for the

TABLE 1. Parameters of original pulser components.

COMPONENT	ESTIMATED WEIGHT (lb)	ESTIMATED DENSITY (gm/cm^3)	ESTIMATED VOLUME cm^3	ESTIMATED EFFICIENCY (%)	AVERAGE POWER AVAILABLE AT OUTPUT (kW)	OUTPUT ENERGY TRANSFER PER PULSE 10 Hz (JOULES)	PEAK OUTPUT POWER PER PULSE (GW)
PRIME POWER					9.80	980	
AC DC POWER CONVERTER, 25 kV	37.5	2.5	6,800	85	8.34	834	
30 kV 2 f CAPACITOR	15	1.5	4,500	90	7.50	750	
TRIGGERED GAS SWITCH	2.5	1.5	700	98	7.35	735	
TRANSFORMER	100	3.5	13,000	80	5.88	588	
ARTIFICIAL BLUMLEIN AND SWITCH	400	0.15	1,200,000	85	5.0	500	
NET SYSTEM	565	0.21	1,236,500	31			

P7027.66

pulser were changed. In the end, it was decided that the pulser must be capable of producing an output with 500 kV, 10 Ω or lower, 200 ns or longer, and approximately 10% rise time in as compact and lightweight geometry as possible. With that in mind, MRC has produced a design that exceeds the original design goals (except for weight) and nearly achieves the specifications listed for a 10 Ω pulser. The final design, as described in Chapter 4, would be capable of producing 500 kV pulses into 10 Ω with pulse lengths between 100 ns and 150 ns (depending upon the water/ethylene glycol mixture used in the capacitors). The pulser would be 2 ft in diameter by 10.9 ft long from primary capacitor bank to output switch, including housing. The pulser would weigh about 1,300 lbs. Most interestingly, though, is that the pulser design allows adjustment for different load impedances. By simply changing-out the inductors of the PFN, the output impedance and pulse length can be changed to almost any value between 10 and 50 Ω.

2.0 ALTERNATIVE DESIGNS

The first activity of the design study concentrated upon examining and comparing different circuit designs for the high voltage section of the pulser. Two classes of circuits were examined: Guillemin voltage fed pulse-forming networks and slow wave structures. The criteria for comparisons not only included electrical, size, and weight performances but also potential problems associated with operations (e.g., charging of the circuits) and difficulties of fabrication and cost management.

Two additional approaches to the design of compact pulsers became apparent during the course of the study. The first approach would utilize high dielectric constant materials in pulse-forming line geometries to achieve the desired compactness. Fabrication of both ceramics (Ref. 4) and plastics (Ref. 5) with high dielectric constants has been demonstrated. However, these materials are probably several years away from use in laboratory pulsed power sources and even further away from use in airborne or spaceborne applications. The second approach would directly drive a load with a transformer. This would eliminate the high voltage pulse-forming line or network. All of the pulse shaping would be performed by a network on the primary side of the transformer. Initially in this design study, fast rise time was an important output parameter. The inductance associated with a transformer was believed to restrict the fast rise time. Recent results, however, indicate that fast rise times are possible with this approach.

2.1 Guillemin Networks

During World War II Ernst Guillemin developed several passive electrical networks for producing rectangular voltage pulses of any desired pulse lengths or impedances (within the limits of realistic element values) (Refs. 2, 6). Guillemin networks have been utilized in pulsed power systems and modulators since their invention. However, no one has attempted to develop them for very high voltage pulsers (above a few hundred kilovolts). The five basic Guillemin networks are shown in Figure 4. For a pulse of impedance Z and pulse length τ, the inductor values are calculated by multiplying the factors for the inductors by $Z\tau$ and the capacitor values are calculated by multiplying the factors for the capacitors by τ/Z. The networks are canonical realizations of each other. In fact, the most basic realization, not shown in Figure 4, involves several LC series resonant circuits connected in parallel. The resonances of the LC sections of this most basic network drive the load at the frequencies of the lower order Fourier components of the voltage pulse. That is, the Guillemin networks mock the important frequencies necessary for a rectangular pulse. It can be shown that only the first five frequency

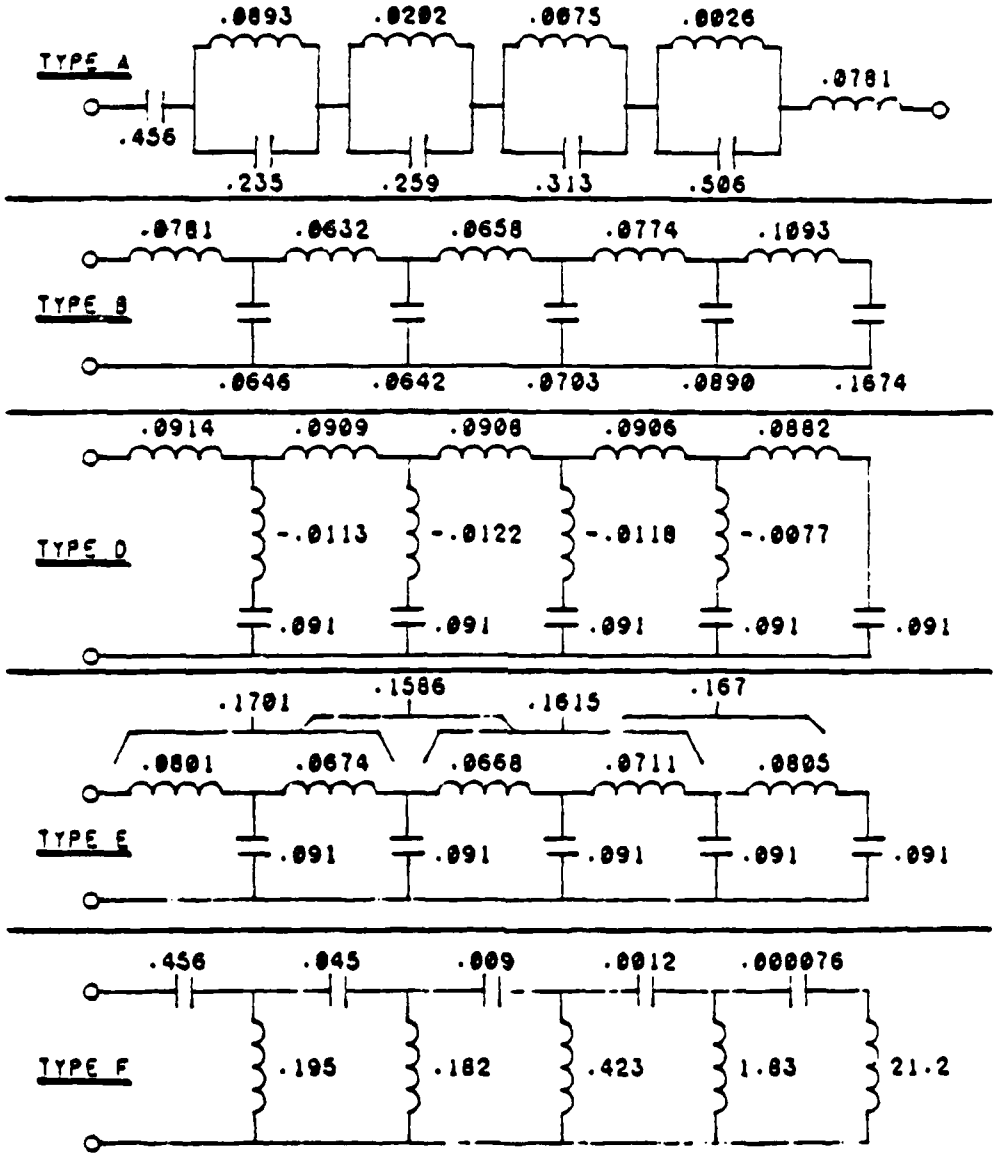

VG-0959

Figure 4. Guillemin pulse-forming networks.

components are necessary for a pulse with a rise time that is approximately 8% of the pulse length. Consequently, only five LC sections are necessary for a network with an 8% rise time.

From Figure 4 it is obvious that the Type D is not realizable since negative inductor values are necessary. However, the Type E network is actually another realization of the Type D where the negative inductors have been replaced by mutual inductances or transformers. For a compact high voltage system, the mutual inductances present an unnecessary complication, especially when considering the Type B network. The Type E network, however, allows constant capacitor values from one stage to the next, and, indeed, many radar modulators are constructed from the Type E. Since the capacitors imagined in this design study may be adjusted to any value, the constant capacitance values of the Type E are of no significant advantage.

Both the Type A and Type F orient the capacitors such that they are stacked in series, so to speak, and parallel with the load. This suggests the possibility of operating these PFNs in a Marx generator like arrangement. Figure 5 illustrates a Type F in a Marx like configuration. The capacitors could be charged in parallel at low voltage through charging resistors or, as in Figure 5, inductors. At peak charge, switches between the stages of the PFN would be closed with a resulting rectangular pulse at the load. This would have the obvious advantage of reducing the voltage required to charge the PFN. Unfortunately, the Types A and F networks require large variations in either or both of the inductor and capacitor values from the first to the last LC section. In practice, such variations are difficult to construct. Additionally, the capacitors are difficult to physically layout in a compact geometry. The capacitors must be stacked along the long axis of the pulser housing. Since the housing must be at ground potential (for equipment and personnel safety external to the pulser), the electric field effects at the edges of the capacitors become difficult to maintain below breakdown levels. This problem is further compounded by placement of the inductors near the capacitors.

The only Guillemin network remaining is the Type B. This type has reasonable component values and has no negative or mutual inductances. The Type B also lends itself well to construction in a compact fashion. One side of all of the capacitors can be a common conductor acting as the PFN ground. As will be shown below, for these reasons, the Type B was chosen as the PFN for the pulsed power source.

2.2 Slow Wave Structures

Slow wave structures (SWS) have been proposed as PFNs for pulsed power machines (Ref. 7). Slow wave structures act in a distributed parameter fashion to reduce

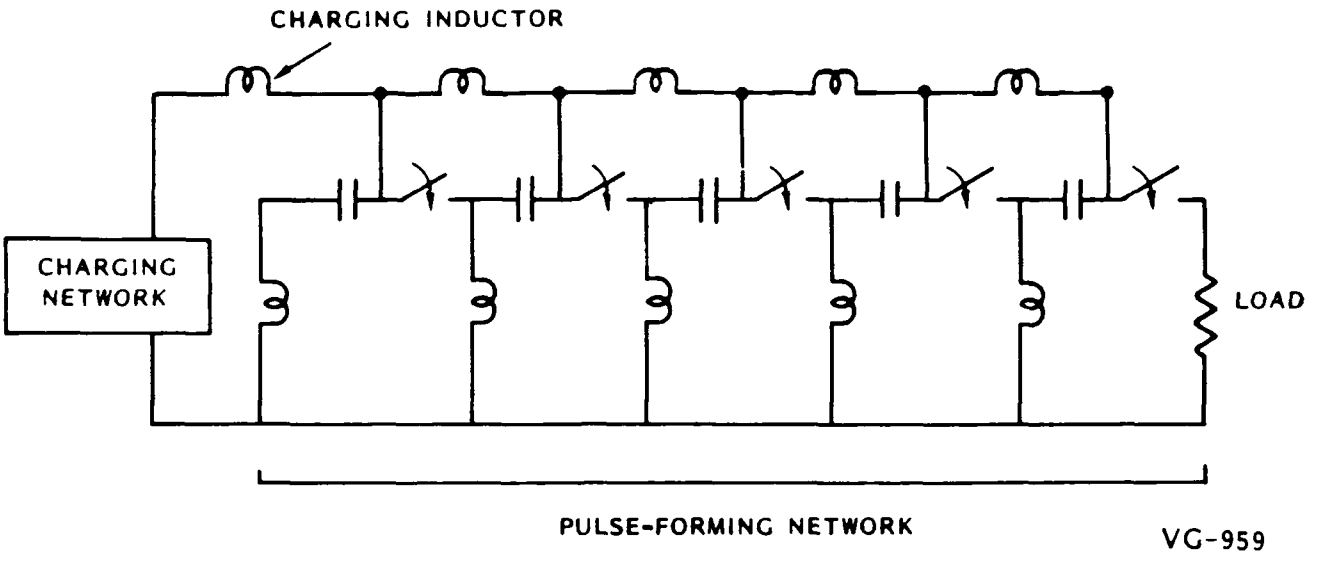

Figure 5. Guillemin Type F network in a Marx-like configuration.

the speed of light in a circuit (Ref. 8). Typically, a structure is built which requires electromagnetic waves to travel a convoluted route requiring more time for the waves to travel the convoluted path rather than a straight path. Consequently, the SWS acts as a delay line. For example, many SWSs are built in a coaxial geometry with a helical inner conductor. To first order, the electromagnetic waves in the helical SWS are forced to follow the path of the helix. Thus, the time required for the waves to travel from one end of the helix to the other is longer than the time required for a wave to travel a path parallel to the axis of the helix.

As with transmission lines or PFNs, SWSs can be used as energy storage devices. Typically, the impedance of SWSs will be proportional to the electromagnetic wave velocity in the circuit. Thus, for pulse-forming SWSs are only suited for high impedance outputs. Unfortunately, SWSs are dispersive to electromagnetic waves. For pulse generation, poor flat tops are produced. Since a pulse is composed of different frequency components, a SWS allows different frequency components to arrive at the load at different times in the pulse. The result is a pulse with large voltage excursions at the end of the pulse. In order to reduce this effect the convolution of the SWS would have to be tapered or tailored in a specific way. This would require on the order of 100 individually fabricated parts per PFN. Additionally, there are some questions related to the dielectric strength of the SWS. The convoluted structures can require edges and spacings between the edges where voltage stand-off become difficult for fractional megavolt devices. As a result of these difficulties associated with the SWS and their impedance characteristics, SWSs were ruled-out as candidates for the design of this program.

3.0 THE EIGHT-HUNDRED JOULE DESIGN

This chapter describes the design which achieved the original design goals outlined in the first chapter. These goals correspond to an output energy of 500 J per pulse. However, the final design described here produced closer to 800 J as the result of a slow pulse fall time.

3.1 Network Design

Based upon the results of comparing the alternative circuit designs, a Type B Guillemin PFN was chosen as the circuit for the Blumlein. In order to reduce the number of inductors with their corresponding volume, an attempt was made to reduce the number of LC sections for the PFN. The energy storage was to be held constant by increasing the capacitances. The number of LC stages was reduced from 5 to 2 per Blumlein side (i.e., the total number of stages was reduced from 10 to 4). This was accomplished by synthesizing (Ref. 2) a Type B Guillemin network with a 33% rise time (i.e., 33% of the pulse length).

A network of two LC series tank circuits connected in parallel was developed. The current from one such tank circuit is given by:

$$i_v = V_N \sqrt{\frac{C_\nu}{L_\nu}} \sin\left(\frac{t}{\sqrt{L_\nu C_\nu}}\right) \quad , \tag{1}$$

where i_v is the current in the tank, ν is the stage or section number of the tank circuit, V_N is the PFN output voltage, t is time, C_ν is the stage capacitance, and L_ν is the stage inductance. Now the Fourier series of a pulse train beginning at time zero (an odd function) is given by:

$$i(t) = I_\ell \sum_{\nu=1}^{\infty} b_\nu \sin\left(\nu\pi t/\tau\right) \quad , \tag{2}$$

where τ is the pulse width, I_ℓ is a the PFN output current, and:

$$b_\nu = \frac{2}{\tau} \int_0^\tau \frac{i(t)}{I_\ell} \sin\left(\nu\pi t/\tau\right) dt \quad . \tag{3}$$

The values of the capacitances and inductances were determined by matching the coefficients for the terms in the Fourier series and the tank circuit currents. Thus, the parameters may be expressed as follows:

$$Z_N = V_N / I_\ell \quad , \quad L_\nu = \frac{Z_N \tau}{\nu \pi b_\nu} \quad , \quad C_\nu = \frac{\tau b_\nu}{\nu \pi Z_N} \quad . \tag{4}$$

The integral for b_ν was evaluated for pulses with parabolic rise and fall of 33% of the pulse width. That is the current of the PFN was specified to be:

$$\frac{i(t)}{I_\ell} = \begin{cases} \left(2\frac{t}{a\tau} - \frac{t^2}{a^2\tau^2}\right) , & 0 \le t \le a\tau , \\ 1 , & a\tau \le t \le \tau - a\tau , \\ \left[1 - \left(\frac{t-\tau+a\tau}{a\tau}\right)^2\right] , & \tau - a\tau \le t \le \tau , \end{cases} \tag{5}$$

where a is the rise time and fall time of the pulse. In this case a was 0.33.

The parallel series resonant circuit was then converted to the ladder network of the Type B form by alternately removing poles and zeros at infinity of the complex frequency space of the PFN's driving point impedance (first Cauer form Ref. 9). The result was the circuit shown in Figure 6. Although the purely reactive PFN circuit would only produce 33% rise times, the addition of the bypass resistors to the last inductors of the Blumlein produced fast rising pulses in the circuit simulations.

The overall circuit design for the 100 Ω pulser is shown in Figure 6. As with the original proposal design, stray reactances are shown at the load. Additionally, inductances of the bypass resistors were added. Figures 7 and 8 show the simulated output pulse with different voltage and time resolutions for the circuit of Figure 6. Excluding the initial voltage drop after the fast rise, the voltage flat top varied by no more than 7% over the 200 ns pulse. The rise time was less than a nanosecond. However, this very fast rise was the result of the 30 pF stray capacitor on the Blumlein side of the prepulse switch. When this 30 pF capacitor was removed, the rise time corresponded to the slower second (about 20 ns) rise as seen in Figures 7 and 8. This slower rise was the L/R exponentiation time of the bypass resistors in series with their inductances (100 nH) and the load and its inductance (25 nH).

Once the Blumlein circuit had been designed, attention was turned to the values and sizes of the various charging and isolation inductors of the Blumlein. The various inductors are shown in Figure 9. The capacitors of the Blumlein (C_{PFN}) are charged

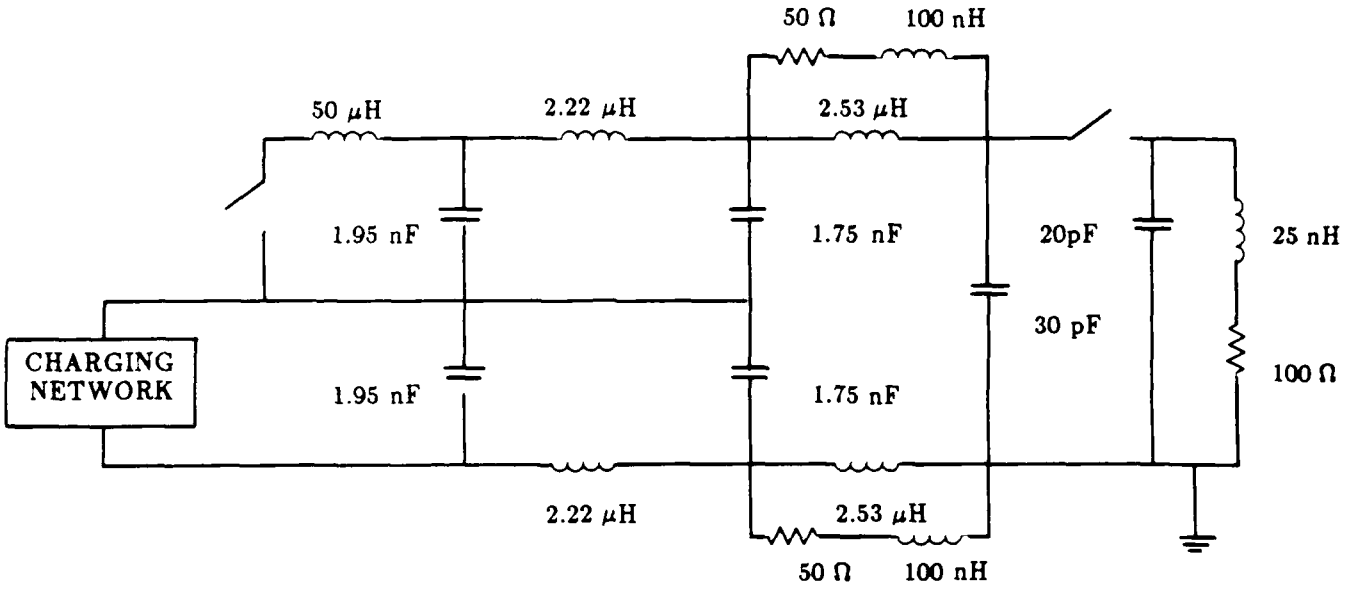

Figure 6. Blumlein pulse-forming network.

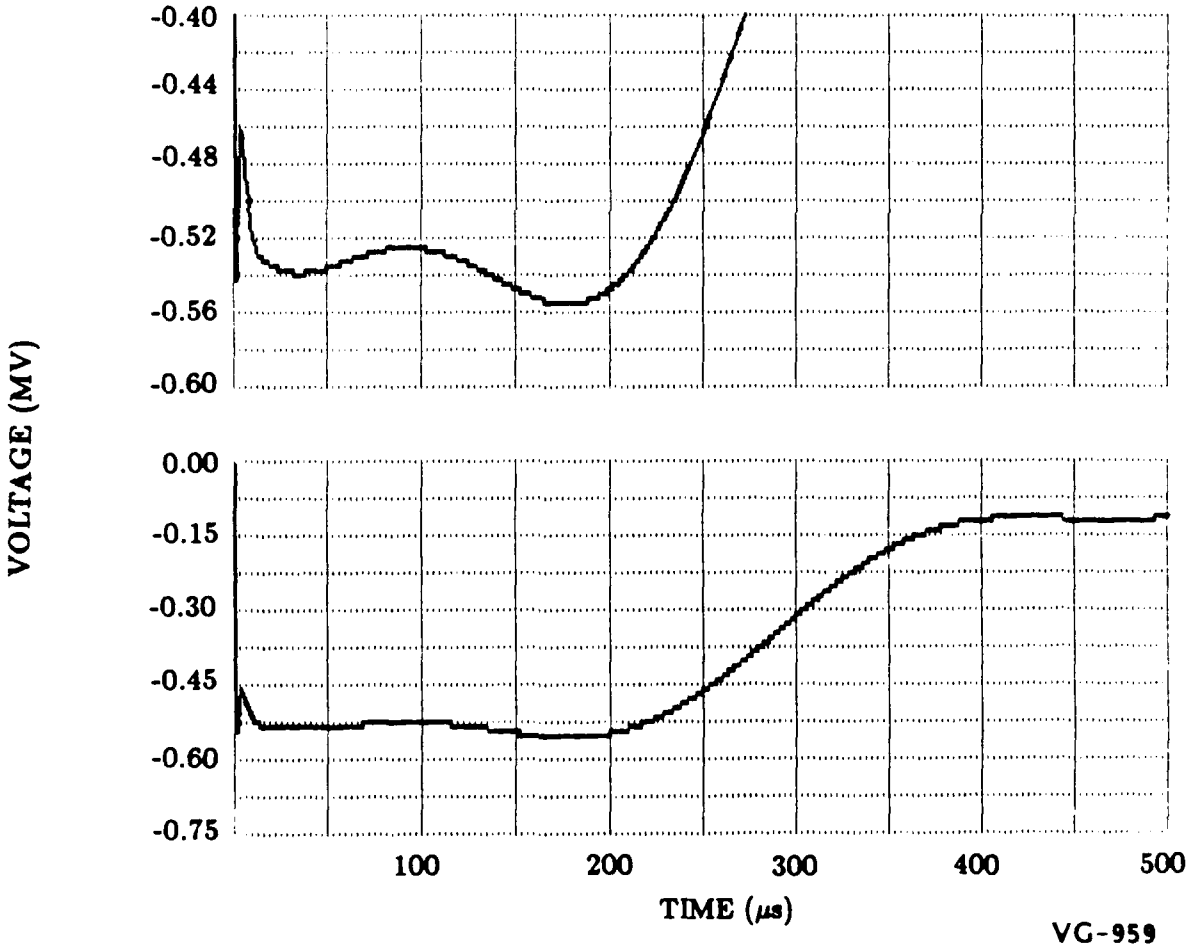

Figure 7. Blumlein output voltage.

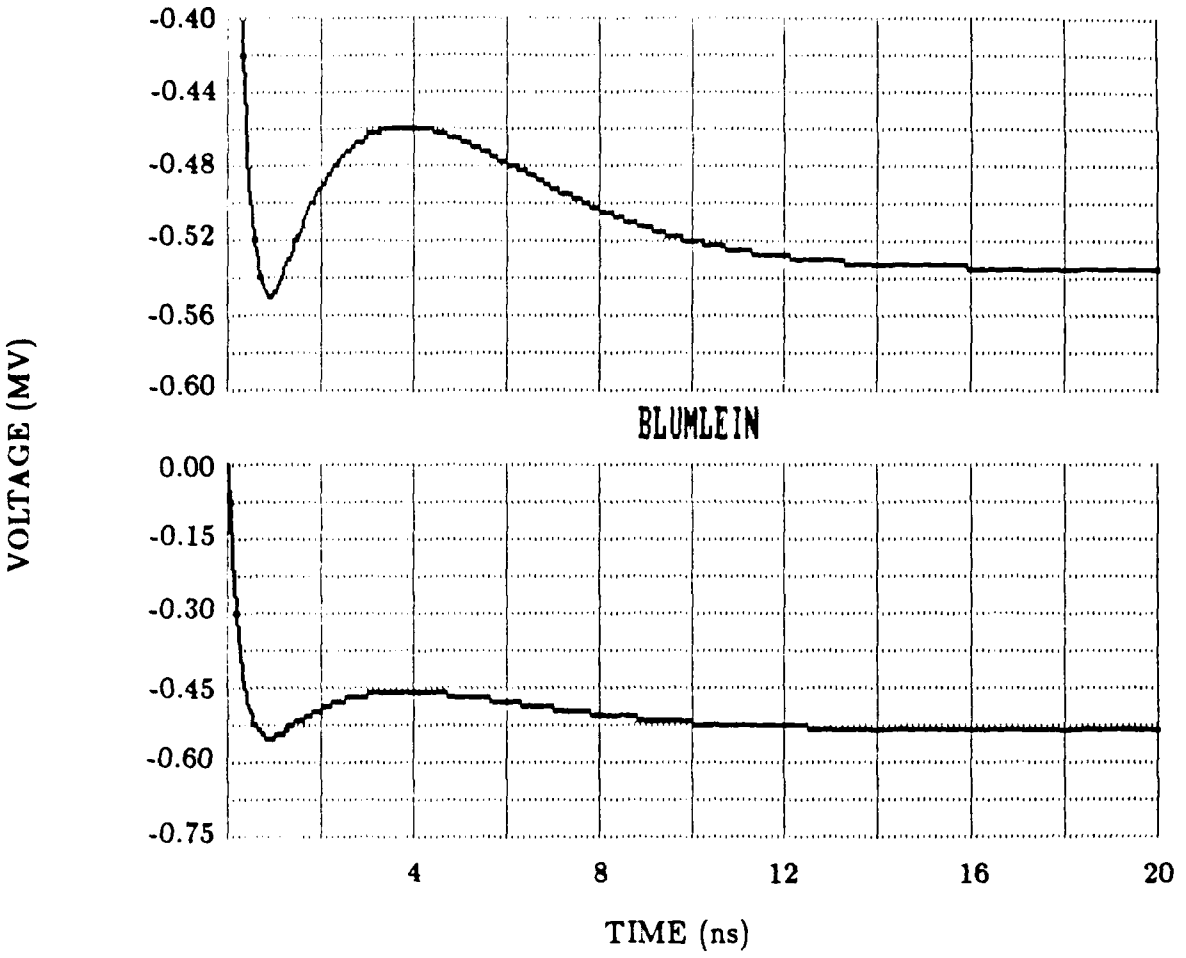

Figure 8. Blumlein output voltage on a smaller time scale.

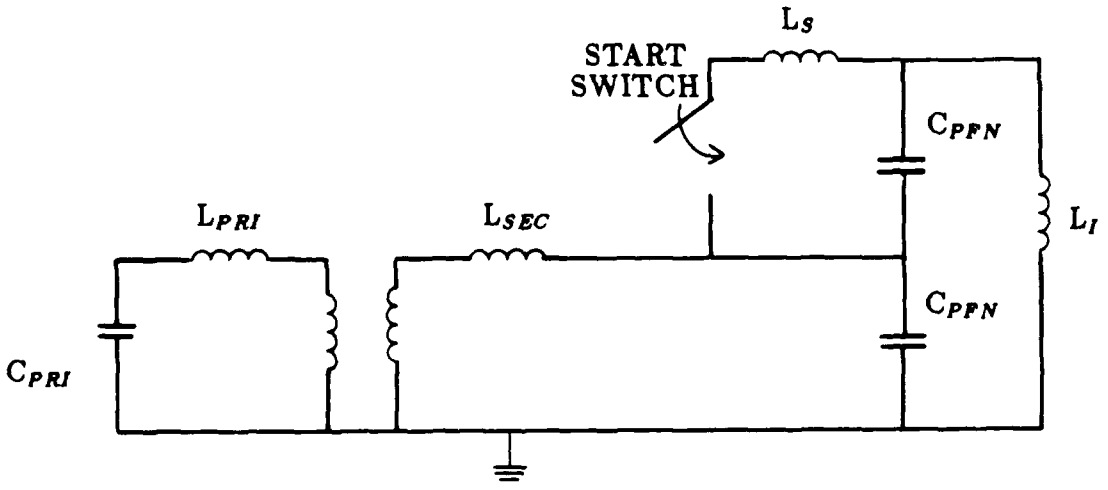

Figure 9. Simplified charging circuit schematic.

VG-959

through a transformer by dual resonance charging from capacitors on the transformer's primary side (C_{pri}). The transformer has inductances associated with its primary (L_{pri}) and secondary (L_{sec}) sides. One condition for maximum energy transfer from one side of the transformer to the other side is that the resonant frequencies of the primary and secondary sides be equal. If L_I is small this resonance condition may be expressed as:

$$\frac{1}{\sqrt{L_{pri}C_{pri}}} = \frac{1}{\sqrt{L_{sec}2\ C_{PFN}}} \quad , \tag{6}$$

or:

$$L_{pri}C_{pri} = 2\ L_{sec}C_{sec} \quad . \tag{7}$$

An isolation inductor (L_I) must be placed between the two sides of the Blumlein so that both sides reach full charge. In Figure 9 the isolation inductor maintains the upper side of the upper Blumlein capacitor (the upper C_{PFN}) at ground potential during charging of the Blumlein. Since the upper capacitor will essentially invert its voltage polarity when the start switch is closed, the isolation inductor must appear as an open circuit during the output time of the pulser. These conditions for the isolation inductor may be written as:

$$\omega L_I \ll \frac{1}{\omega C_{PFN}} \quad , \tag{8}$$

or:

$$\omega \ll \frac{1}{\sqrt{L_I C_{PFN}}} \quad , \tag{9}$$

and:

$$\frac{2\pi L_I}{\tau} \gg Z_{PFN} \quad , \tag{10}$$

where τ is the pulse length of the PFN, and Z_{PFN} is the output impedance of the PFN.

In order for the Blumlein to operate, the voltage of the upper PFN in Figure 9 must invert. This is accomplished by an inductor, referred to here as the swing inductor,

in series with the start switch (L_S). The upper PFN capacitor and the swing inductor oscillate as a parallel LC circuit. The oscillation period of the PFN capacitor and the swing inductor must be larger than the pulse length of the Blumlein. Otherwise, the oscillation of the PFN capacitor and the swing inductor is imposed upon on the Blumlein output. This may be expressed as follows:

$$\sqrt{L_S C_{PFN}} \gg \tau \quad , \tag{11}$$

or:

$$L_S \gg \frac{\tau^2}{C_{PFN}} \quad . \tag{12}$$

Additionally, the swing inductor must be much smaller than the isolation inductor so that the voltage on the upper PFN inverts before any charge can be depleted through the isolation inductor ($L_I \gg L_S$).

All of these conditions can be combined and written as follows:

$$L_{sec} \gg \frac{L_I}{2} \gg \frac{L_S}{2} \gg \frac{\tau^2}{2C_{PFN}} \quad . \tag{13}$$

Now if one allows $\gg$ to mean 5 times greater than and since $\tau = 200$ ns and $C_{PFN} = 3.7$ nF, the values for the inductors become:

$$L_S = 54\ \mu H \ , \quad L_I = 270\ \mu H \ , \text{ and } \quad L_{sec} = 675\ \mu H \quad . \tag{14}$$

The value for the transformer secondary is within the range of such transformers, and the swing inductor value is larger than desirable but not unreasonably large. However, the isolation inductor value for the high voltages it must stand-off was deemed too large for a compact system.

Two additional disadvantages of the Blumlein arrangement became apparent. First, although the Blumlein is charged to the output pulse voltage, the voltage inversion necessary for one PFN of the Blumlein requires the same voltage stand-off as the a conventional PFN (twice the output voltage). This is particularly true for long pulse length sources where delay times of breakdown events cannot be utilized to enhance the stand-off voltages of the pulser components. Blumlein operations provide an advantage

where power supply voltages are limited. (Not a problem in this case.) Second, the Blumlein has two additional inductors and an additional switch that a simple PFN pulser would not. Although, these components present no real problem (except for the isolation inductor) they do reduce simplicity and would reduce reliability. Consequently, the Blumlein configuration was abandoned and a straight PFN circuit was adopted.

The resulting 100 Ω pulser circuit is shown in Figure 10. The PFN design is the same as that for the Blumlein. However, the impedance of the straight PFN is twice that of the PFN arms of the Blumlein design. Consequently, the inductor and capacitor values are different. Figure 11 shows the simulated output of the PFN. Again, the initial fast spike at the beginning of the pulse was the result of the stray 30 pF capacitor discharging into the load. However, the flat top of the pulse only varied by 9%. The better flat top performance was the result of two effects. A Blumlein operates by essentially allowing one side of the Blumlein to change voltage polarity and then stack the outputs of the two PFNs or transmission lines in series. Thus, any voltage variations in the individual arms of the Blumlein design were multiplied by two in the output of the Blumlein since the two arms are exactly alike (i.e., have the same driving point impedance). Second, the inductance of the bypass resistor was reduced by eliminating the large loop in the stage of the PFN nearest the load in the Blumlein. Consequently, the L/R time of the bypass resistor loop was smaller.

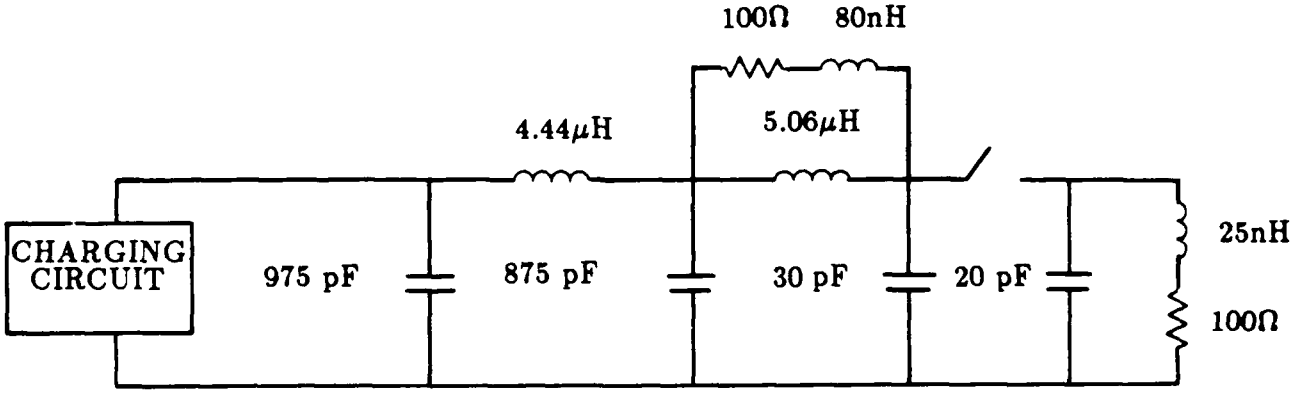

Figure 10. Network schematic of 800 J PFN.

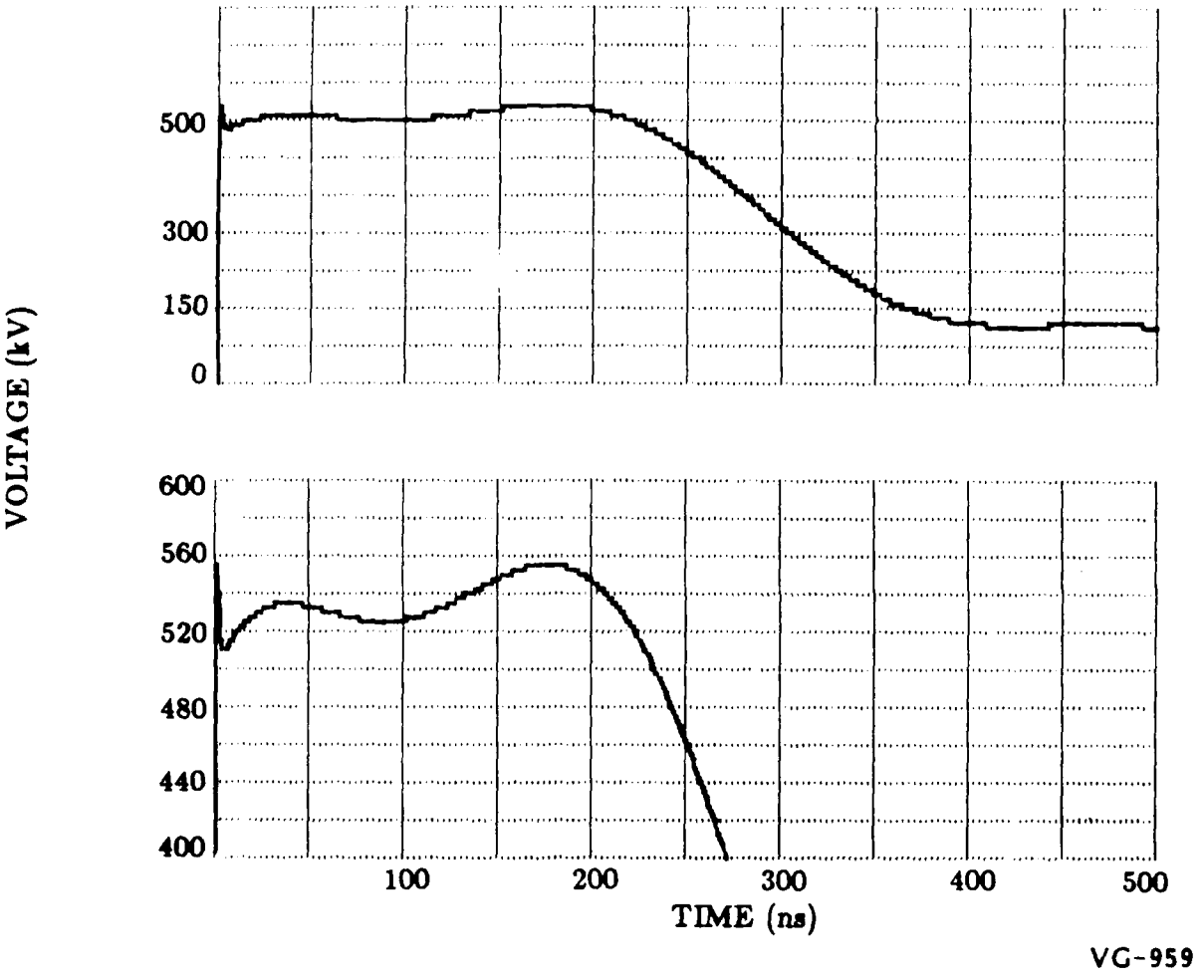

Figure 11. Simulated output voltage of 800 J PFN.

Figures 12 through 14 show additional simulations of the design. Figure 12 illustrates the energy and power performance of the 100 Ω pulser. The energy and power are presented in negative values since these parameters represented extracted values. Normally, a 500 kV, 200 ns pulse would produce 500 J of energy. However, the slow fall time of the pulser provided an additional 300 J. The energy consumed by the bypass resistor was a modest 11% of the output energy, as seen in Figure 13. For a low energy, repetitively pulsed source, as the 100 Ω design is, the waste energy of the bypass resistor is difficult to manage. Finally, Figure 14 shows the voltage on the PFN capacitors during charging and the PFN output voltage on the same time scale.

3.2 Component Design

Based upon the results of the circuit design, an attempt was made to design the PFN components utilizing a flat plate geometry. An electrostatic field solving code, JASON (Ref. 10), was used to determine the electric field values within the capacitors. These field levels were then compared to known or calculated field breakdown levels in the media of the components. Dimensions were forced as small as breakdown limits would allow.

Early JASON calculations indicated that the flat plate geometry would be difficult to implement. Large field enhancements at the plate edges would have required very careful grading of the fields at the edges. Such grading would have involved a gradual flaring of the capacitor edges with an increase in the PFN volume. Additionally, the flat plate configuration appeared difficult to mount in some reasonable housing. For equipment protection and personnel safety, the PFN must be placed in a conducting housing. Such a housing presented an electrical breakdown problem between the high voltage plates of the PFN and the housing. Also, the housing produced stray capacitances between the high voltage side of the PFN and the housing (ground) with a consequential degradation in the electrical performance of the pulser.

Alternatively, a coaxial geometry eliminated these problems. The housing could then act as the ground side of the capacitors, while the inner conductor of the coax could be charged to the PFN charging voltage. The stray capacitances were also folded into the shape of the coax. As a result the component designs were converted to coaxial geometries. Figure 15 shows the overall layout of the 800 J pulser in its cylindrical form.

Capacitance values were calculated from a standard formula for coaxes (Ref. 11) and is given by:

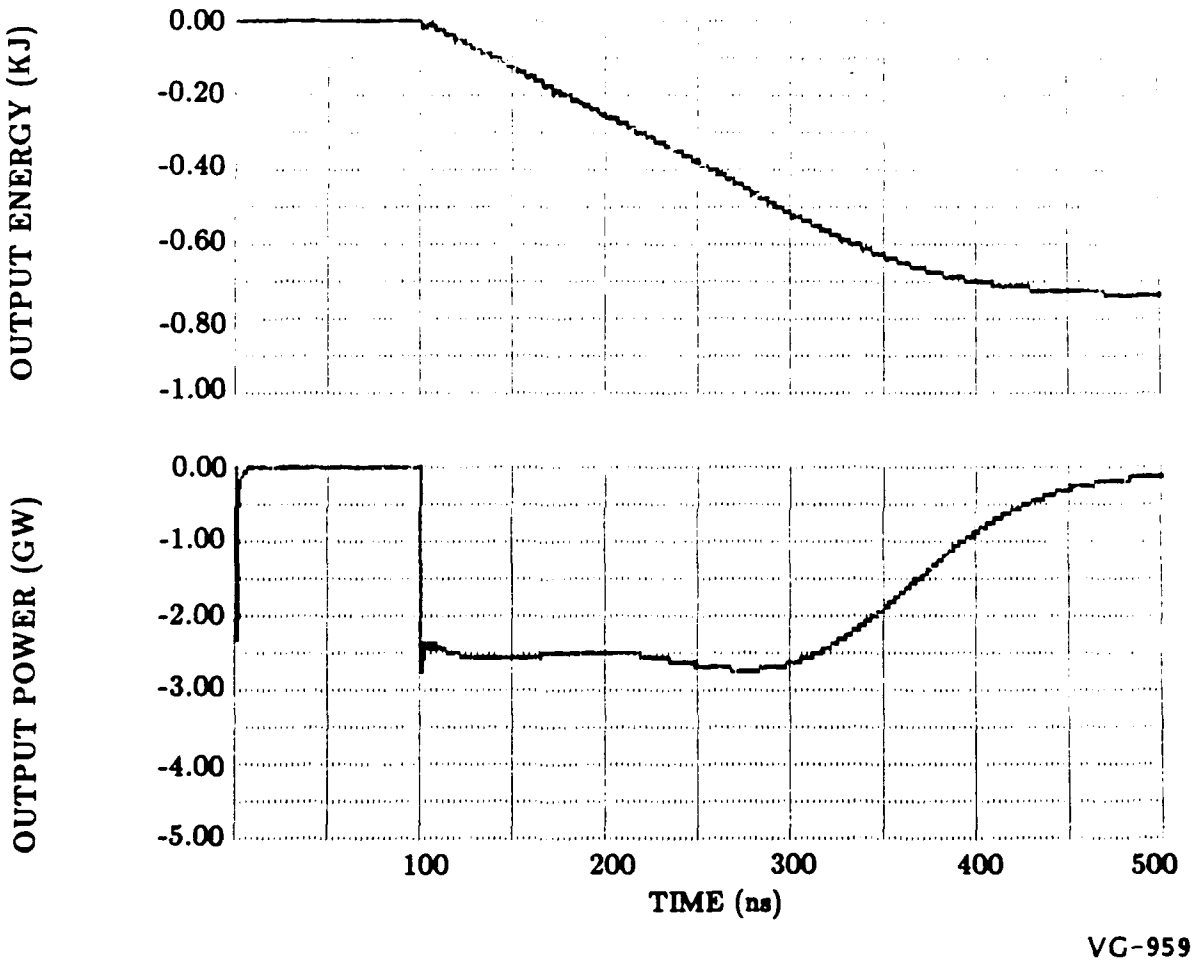

Figure 12. Output energy and power of 800 J design.

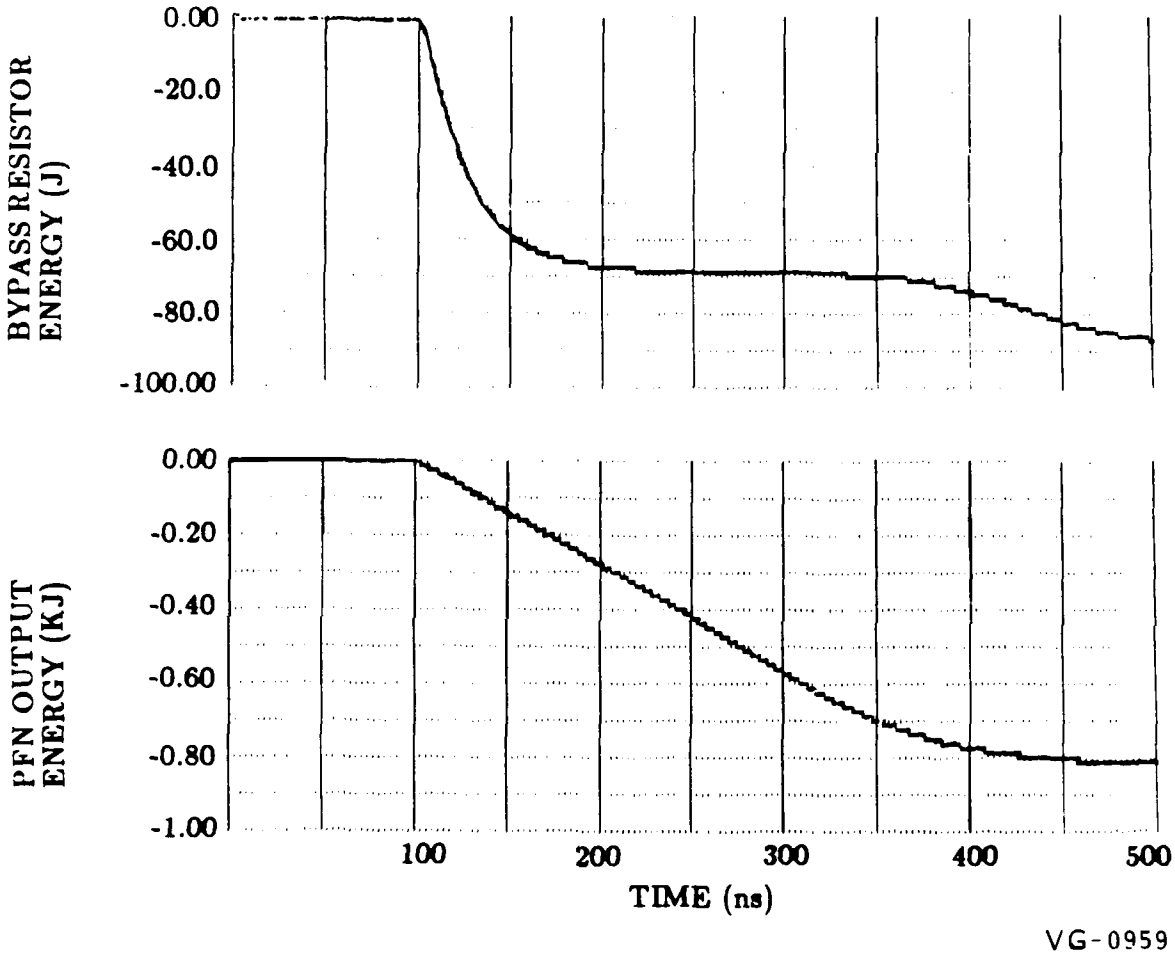

Figure 13. Energy consumed per pulse by the bypass resistor and the output energy of the 800 J design.

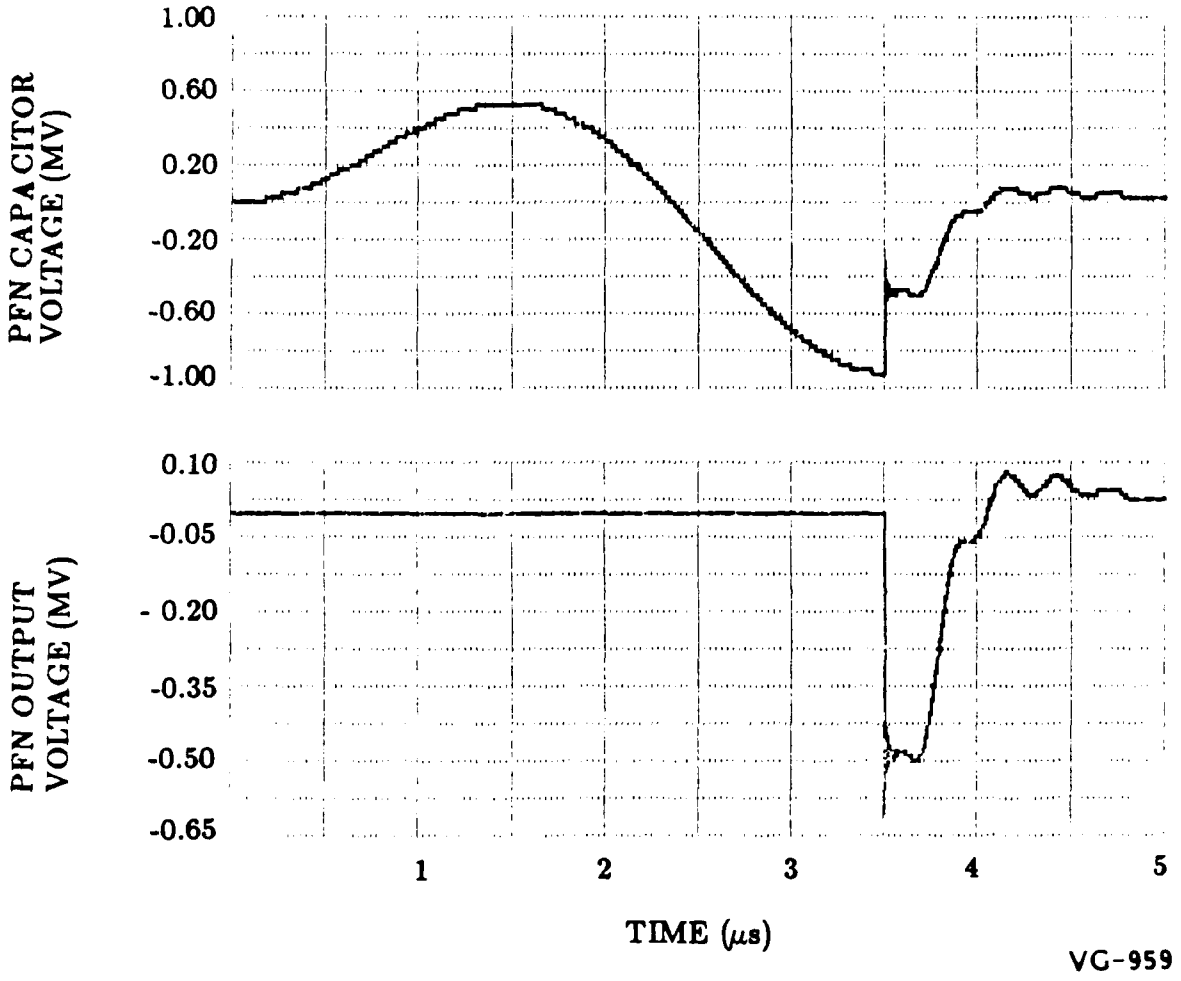

Figure 14. Voltage on one of the PFN capacitors showing the charging of the PFN and the PFN output voltage for the 800 J design.

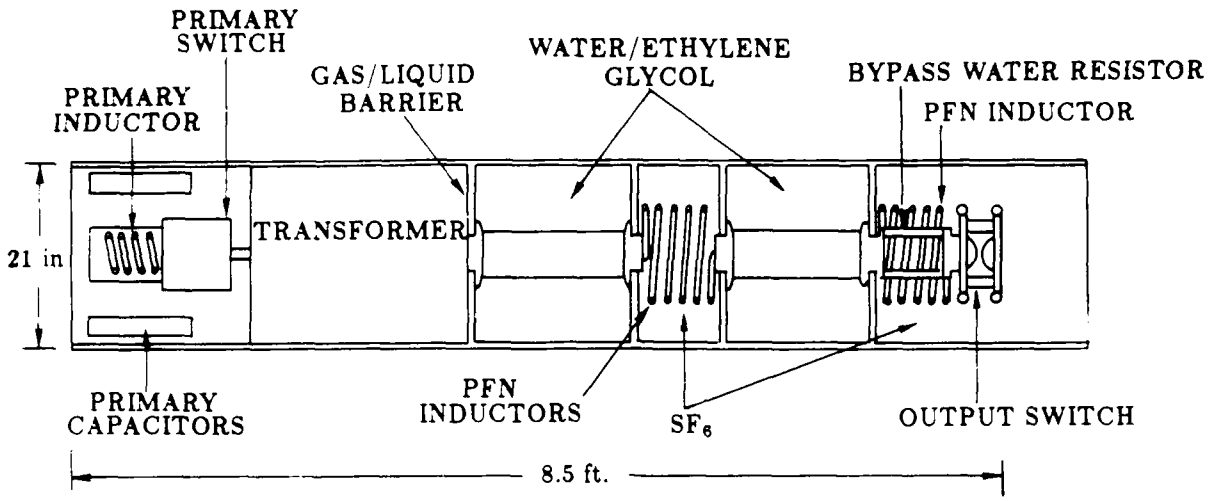

Figure 15. Physical layout of 800 J pulser design.

$$C = \frac{2\pi\epsilon\ell}{\ln(b/a)} \quad , \tag{15}$$

where b is the outer radius of the coax, a is the inner radius of the coax (a and b may be in any units so long as they are in the same units), ℓ is the length of the coaxial region of interest, and ϵ is the permittivity of the capacitance medium. To provide some degree of temperature tolerance, the capacitors were designed with a water ethylene glycol mixture. Glycol is antifreeze and lowers the freezing point of water while also raising the boiling point. However, the glycol also lowers the dielectric constant of water. For the maximum temperature range, a water to ethylene glycol ratio of 40:60 is required. This ratio reduces the dielectric constant of water (Ref. 12) from 80 to 58. (More will be presented on water dielectrics in the next chapter.) The capacitors of the 800 J pulser were designed with a dielectric constant of 58.

Electric field values were calculated according to, again, a standard formula (Ref. 11) by the expression:

$$E = \frac{V}{r\ln(b/a)} \quad , \tag{16}$$

where E is the electric field strength at a specific radius r in the coax, V is the voltage of the capacitor, and b and a are the outer and inner radii, respectively. Now, the breakdown strength of water can be calculated according to Martin (Ref. 13) by:

$$E_{br} = \frac{k}{t_{eff}^{1/3} \; A^{1/10}} \quad , \tag{17}$$

where E_{br} is the electric field breakdown strength in MV/cm, t_{eff} is the effective charging time on the water in μs, A is the area of the electrode in cm^2, and k is a constant which is 0.3 for positive charging or 0.6 for negative charging. The effective time is the time necessary for the charge to change from 63% full charge to full charge. Essentially, the values of k and A are determined by the electrode which has the higher electric fields. For the 800 J pulser, k and A were evaluated for the inner electrode. Some care must be taken with Martin's equation. The equation is an empirically derived expression for single pulse applications. The accuracy of this equation for repetitively pulsed compact water dielectrics is not known. However, Martin's equation is probably not more than a 50% off of its single pulse values.

JASON was utilized to calculate some of the electric field strengths and capacitances of the 800 kJ PFN. These calculations agreed with the results from the analytical expressions described above. However, the JASON calculations were terminated when the emphasis of the study turned to higher energy designs. The JASON results from the 3 kJ design may be adapted to the 800 J design.

Table 2 presents the dimensions of the PFN inductors. These dimensions were obtained from the following formula:

$$L = \frac{N^2 r^2}{(10\ell + 9r)} \quad , \tag{18}$$

TABLE 2. Inductor parameters.

(number of turns = 5 , length = 25 cm)

n	L (μH)	Radius (cm)
1	5.06	12.8
3	4.44	11.8

where L is the inductance of the coil in μH, N is the number of turns, ℓ is the length of the coil in inches, and r is the radius of the coil in inches. More accurate formulae are presented in Grover (Ref. 14) and the formula above agrees within 15% with the formulae of Grover.

4.0 THE THREE/FOUR JOULE DESIGN

Based upon discussions with Air Force personnel, a multi-kilojoule design was attempted. This attempt was based on the same concepts presented in the previous chapter. Basically, a coaxial geometry of alternating water capacitors and gas insulated coil inductors was utilized. The physical design is shown in Figure 16. This design produced approximately 100 ns pulses with a 10 Ω output (i.e., 3 kJ) in circuit simulations. As opposed to the 800 J design, this design does not use a bypass resistor for fast rise time and enhanced flatness of the flat top. At this energy, a bypass resistor would consume an unacceptable amount of energy. Table 3 lists the parameters of the sub-systems of the pulser design including an estimate of the power conditioning (not shown in Figure 16) weight and volume as determined from Appendix B. The 3–4 kJ pulser is estimated to cost $30,000 for a single copy and approximately $15,000 per copy under mass production (without power conditioning, prime power, gases, and fluids).

4.1 Network Design

Without the bypass resistor, the design approach used for the 800 J design had to be altered. In order to maintain a reasonable rise time with an acceptable flatness, a Guillemin PFN with a parabolic rise and fall of a = 0.2 (i.e., a 20% rise time) was synthesized. Such a circuit requires three LC sections in order to have reasonable convergence and acceptable flat top variations. The resulting PFN schematic is shown in Figure 17 without the stray elements.

Extensive simulations were conducted to evaluate and refine the performance of the pulser design. Figure 18 shows the circuit schematic used to simulate the PFN. Since the impedance of the pulser design was low, the capacitors were simulated as semi-distributed elements. This was accomplished by decomposing each capacitor into five capacitors and five inductors in a ladder network. Additionally, realistic parasitic reactances were added to the output of the pulser. These parasitics mostly involved stray capacitances associated with a spark gap output switch and an electron beam diode. Since most stray inductances are in series with the output, the stray inductances may be incorporated into the PFN inductor nearest the load. Circuit simulation results are shown in Figure 19 for the 10 Ω, 100 ns pulser design. The output voltage had a pulse width of 108 ns as measured from the time the voltage first reached -500 kV to the time the voltage last crossed -500 kV. The voltage rose from 0 kV to -500 kV in 12 ns (or 11% of the flat top time) and had a flat top variation of 140 kV (or 28% of 500 kV). Three larger humps in the flat top were associated with the three LC sections of the PFN. The smaller faster oscillations were the result of oscillations (i.e., distributed parameter

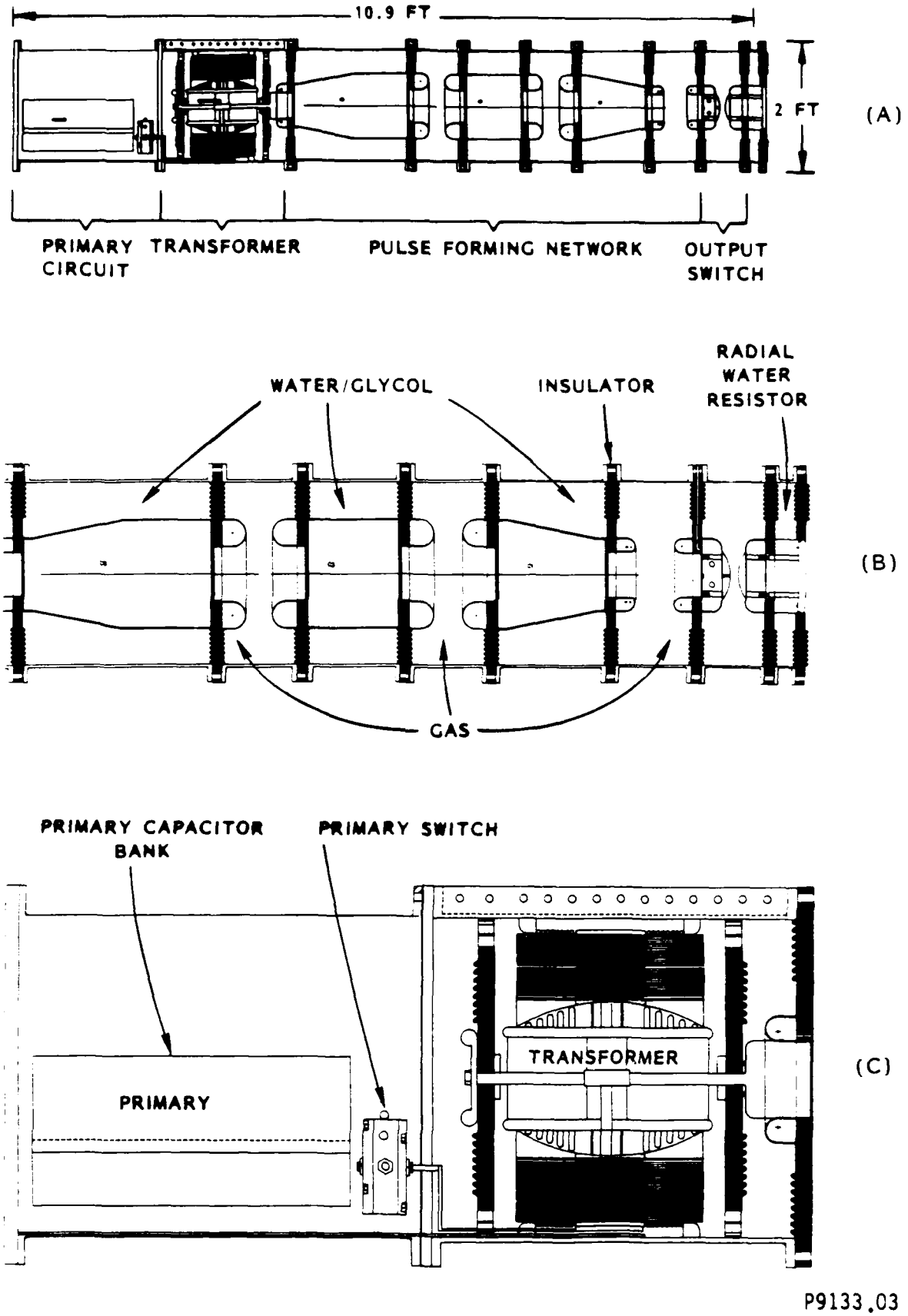

Figure 16. Layout of 3–4 kJ pulser: (A) overall layout (inductors not shown), (B) PFN (inductors not shown), (C) primary circuit and transformer.

TABLE 3. Parameters of 3 kJ pulser components.

COMPONENT	WEIGHT lb (kg)	VOLUME ft^3 (cm^3)	EFFICIENCY %	AVERAGE POWER AVAILABLE AT OUTPUT kW	OUTPUT ENERGY TRANSFER PER PULSE 10 Hz Joules	OUTPUT POWER PER PULSE GW
PRIME POWER				44.3	4430	
POWER CONVERTER, 70 kV	73 (33.1)	0.85 (24,070)	85	37.7	3770	
PRIMARY CIRCUIT	178 (80.7)	6.2 (175,570)	95	35.8	3580	
TRANSFORMER	350 (159)	3.6 (101,940)	90	32.2	3220	
PULSE-FORMING NETWORK	620 (281)	22.3 (631,470)	95	30.6	3060	
OUTPUT SWITCH	79 (35.8)	1.2 (33,980)	98	30.0	3000	
NET SYSTEM	1300 (590)	34.2 (967,030)	67.7	30.0	3000	25.0

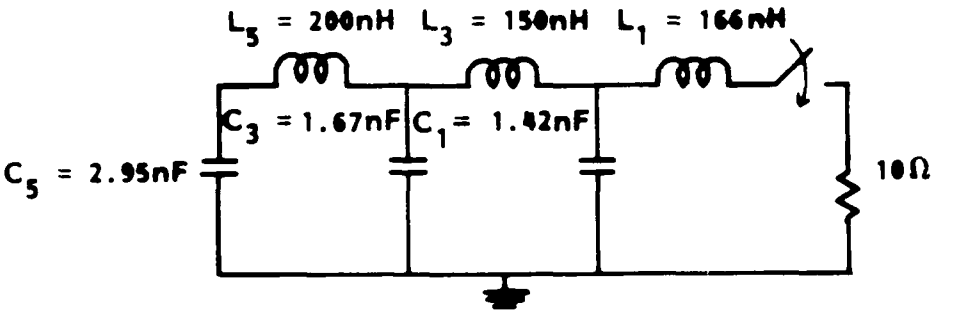

Figure 17. Type B Guillemin pulse-forming network for Phase I design.

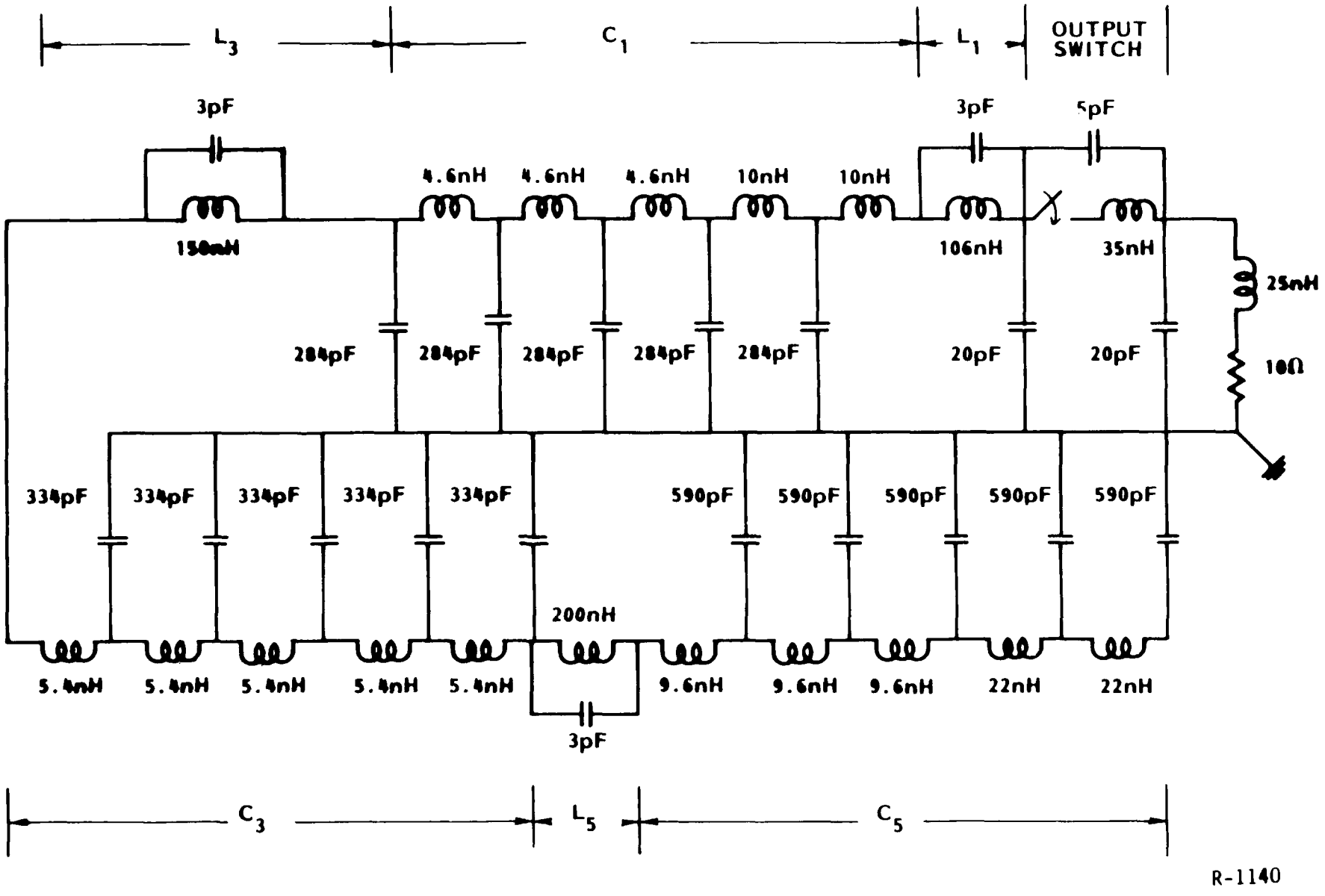

Figure 18. Circuit model for PFN simulations.

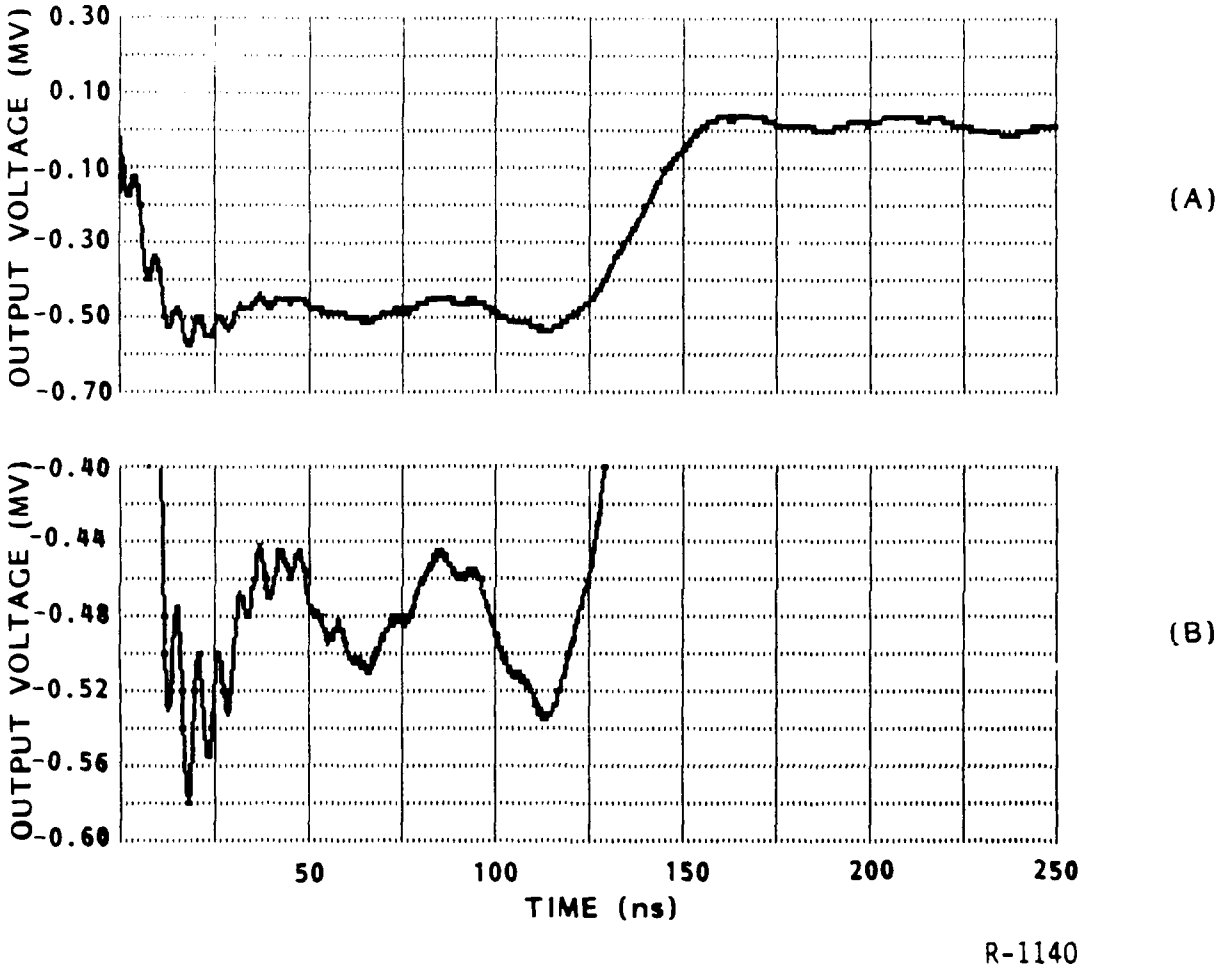

Figure 19. Output voltage of 10 Ω, 100 ns, 3 kJ PFN, (A) full scale, (B) smaller voltage scale.

effects) in the PFN capacitors. Additionally, the stray reactances around the output region of the PFN induced the strong fast oscillations early in the pulse. Figure 20 shows the energy out of the pulser. Since the circuit solving code calculated the energy extracted from the PFN, the energy is presented in negative values in Figure 20.

An important advantage of this PFN design is pulse width and output impedance agility. The PFN design may be quickly and easily converted to higher output impedances and longer pulse widths by changing the PFN inductor values. However, the energy stored by the PFN at peak voltage during charging (or, alternatively, the output energy) must remain at 3 kJ. Thus, the relationship between output impedance and pulse length must not violate:

$$\frac{\tau}{Z} = 1.4 \times 10^{-8} s/\Omega \quad , \tag{19}$$

where τ is the pulse length in seconds, and Z is the output impedance in ohms. The inductor values for a given output impedance are given by the expression:

$$L_n = \frac{k_n}{\tau Z} \quad , \tag{20}$$

where k_n is a constant similar to those shown in Figure 4 and are given in Table 5 for the high energy pulser, n is the subscript associated with the LC section of the PFN, and L_n is the inductance in henries of the LC section for the given impedance. Figure 21 shows a simulation in which the inductors for a 20 Ω output were used. The same circuit schematic as Figure 18 was used except for the change in inductor values. For the 20 Ω case, the small fast oscillations of the 10 Ω case were not present. Since the output impedance was higher, the distributed nature of the capacitors had less of an effect. The 20 Ω pulser had less than a 15% rise time (0 to -500 kV) and less than a 15% flat top variation. As predicted, the output pulse length was increased to 200 ns from first to last crossing of -500 kV.

The pulse width and impedance "tunability" allows any values from 10 Ω, 100 ns to 50 Ω, 500 ns. The distributed nature of the capacitors and the performance degradation associated with the parasitic reactances limit the lower impedance and shorter pulse widths of the pulser. Reasonable inductor values and the superposition of the charging waveform on the output waveform limit the higher impedances and longer pulse lengths. Further, impedance/pulse width agility may be realized by varying the dielectric constant of the capacitor media. The capacitors were designed with a dielectric constant of 58. This was the result of utilizing a water and ethylene glycol mixture to provide a

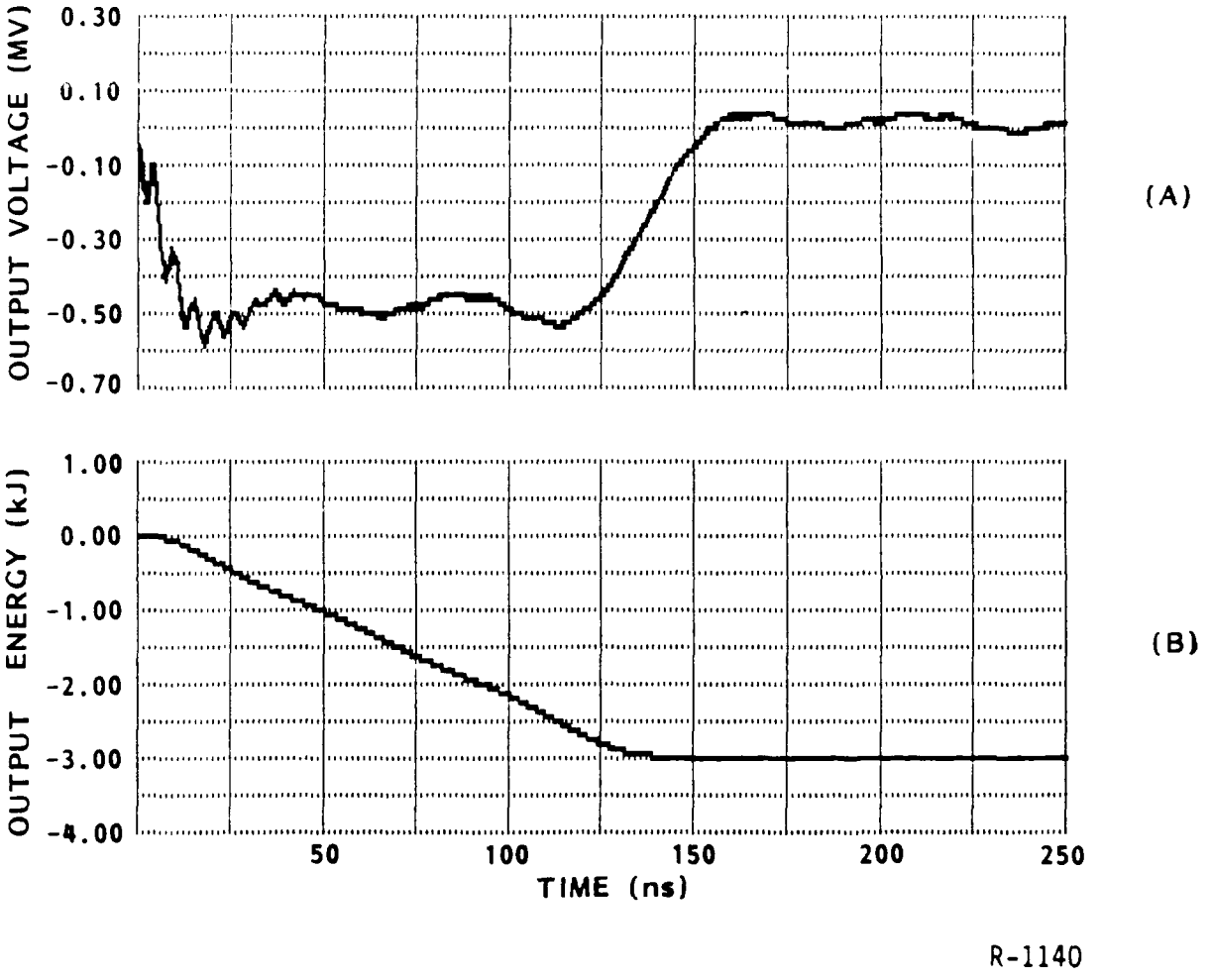

Figure 20. Output voltage (A) and output energy (B) of 10 Ω, 100 ns, 3 kJ PFN.

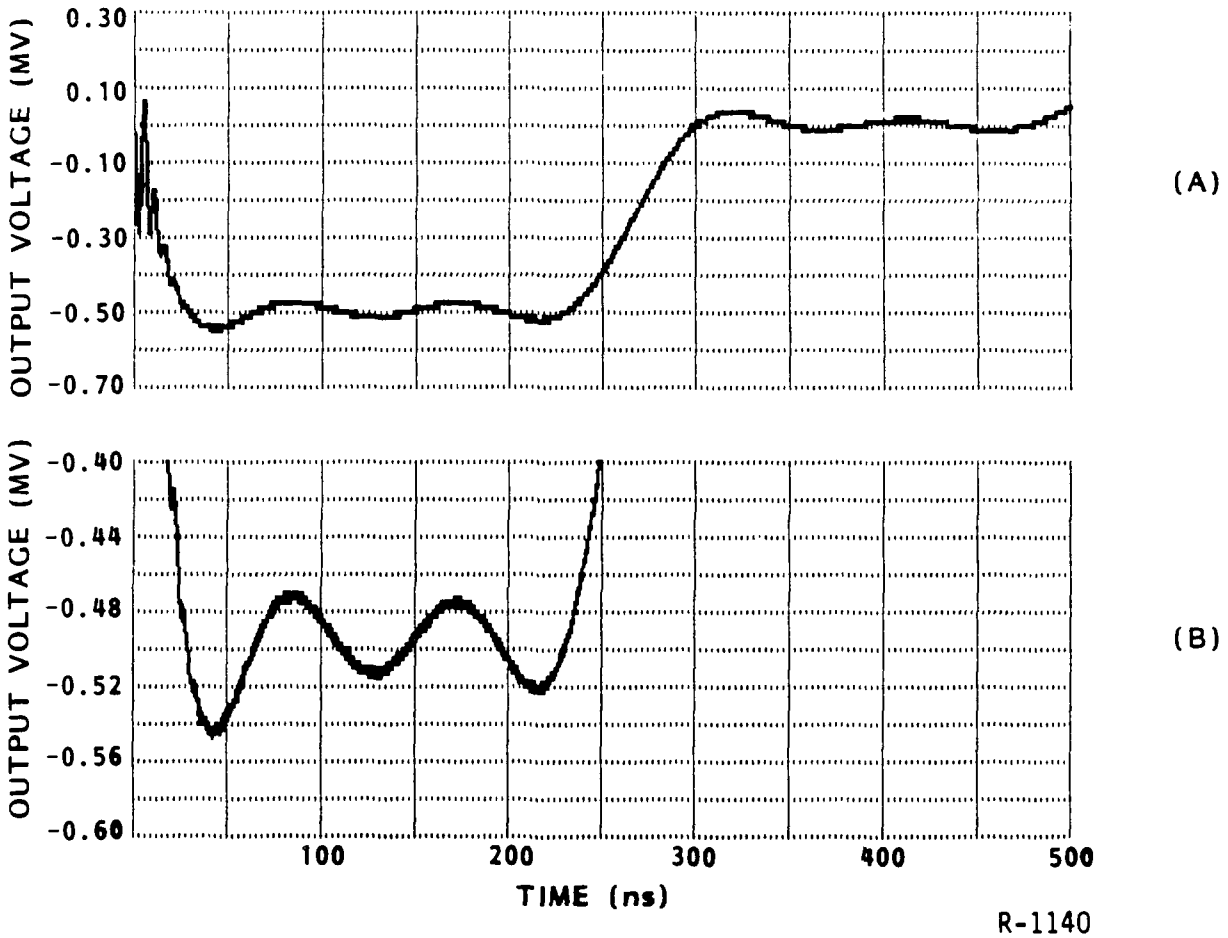

Figure 21. Output voltage of 20 Ω, 200 ns, 3 kJ PFN, (A) full scale, (B) smaller voltage scale.

wider operating temperature range than that of pure water. However, the water and ethylene glycol mixture ratio may be varied to allow a dielectric constant (Ref. 12) anywhere from 40 to 80 but with a reduction in the operating temperature range for ratios other than 40:60 water:glycol. Consequently, the maximum energy that may be stored in the PFN ($\epsilon_r = 80$) is approximately 4 kJ.

This energy would allow a 10 Ω output impedance with a 150 ns pulse length. Figure 22 shows the output voltage when the water capacitor values were increased for maximum energy and 10 Ω output. The waveform is similar to the 3 kJ case but with a longer pulse length. The output energy for the 4 kJ pulser is shown in Figure 23.

A further advantage of this design is its tolerance of high inductance loads. Almost all loads imaginable for this pulser design will have some inductance. For example, vacuum insulator stacks necessary for electron beam devices add inductance to the impedances of the electron beam diodes, or transitions from coaxial to flat plate or strip line geometries are inductive. This inductance tolerance may be realized by allowing the load inductance to act as part of the PFN inductor nearest the load (L_1). To simulate this effect, the circuit of Figure 18 was changed such that the 25 nH inductor of the load was interchanged with the 106 nH of the PFN. The resulting output voltage waveform of the simulation is shown in Figure 24. The increased inductance at the load reduced the oscillations associated with the stray reactances of the output switch and the load.

Thus, this design allows great flexibility in the output parameters. This single design allows a pulser which can be adjusted to the particular application or mission of the device or weapon it drives.

4.2 Component Design

Water was chosen as the capacitor dielectric for a variety of reasons. First, water has a high dielectric constant ($\epsilon_r = 80$ for purified deionized water) which allows high energy storage, low output impedance, and long pulse length. Second, water is a commonly used dielectric in laboratory pulsed power sources. Thus, a fair amount of data is available on the performance of water under high field stresses (Refs. 12, 13, 15, 16, 17, and 18). Third, liquid dielectrics are somewhat fault tolerant. There is almost always a non-negligible probability that breakdown will occur in a medium under high electric field stresses. For a water capacitor this may represent a certain number of breakdowns occurring in the water during a certain number of charging cycles. Water has been shown to recover from breakdowns in times short compared to the repetition rates required for this design (Ref. 18, 10 Hz). However, a capacitor with a solid dielectric would be rendered permanently useless should breakdown occur within the

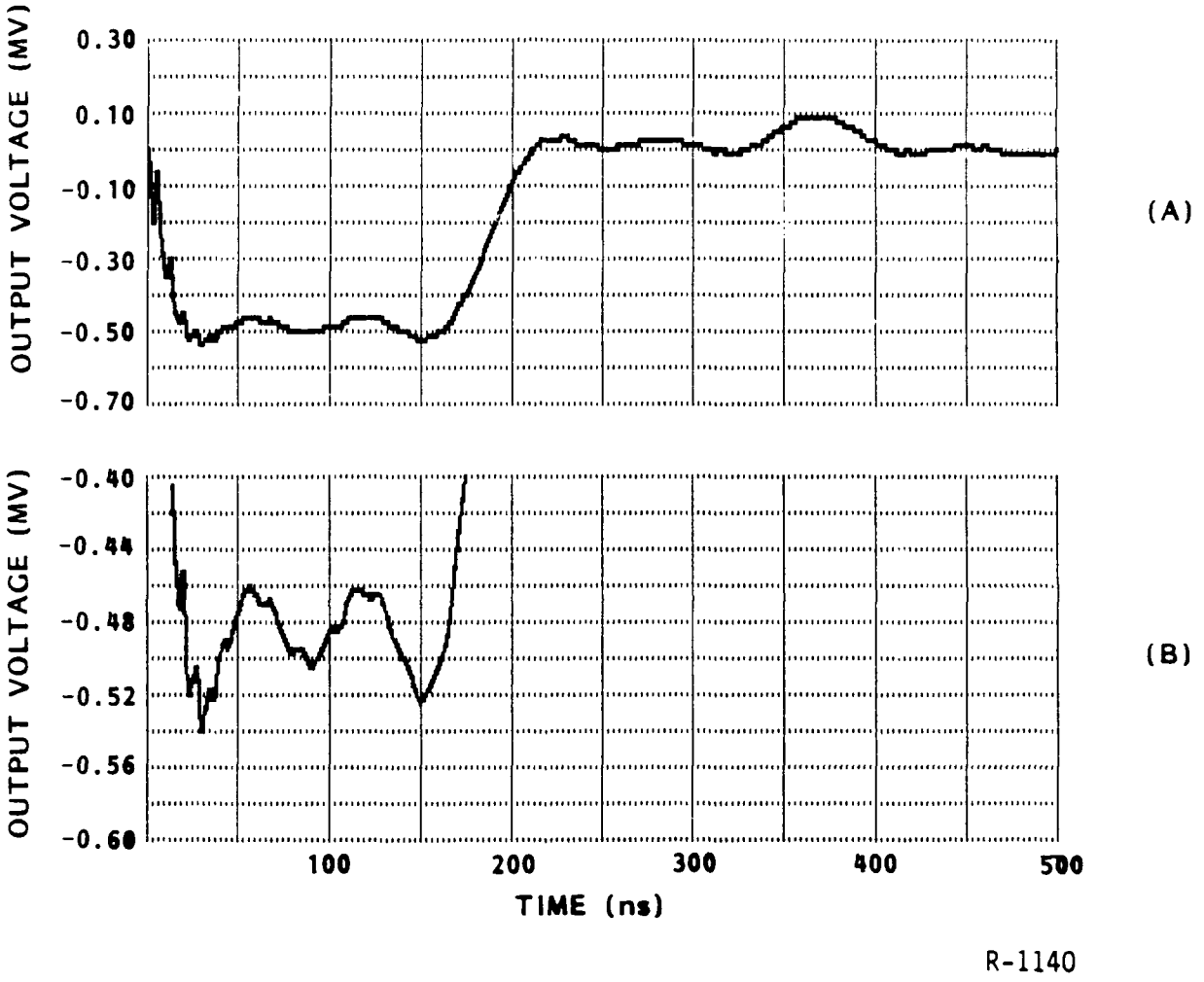

Figure 22. Output voltage of 10 Ω, 150 ns, 4 kJ PFN, (A) full scale, (B) smaller voltage scale.

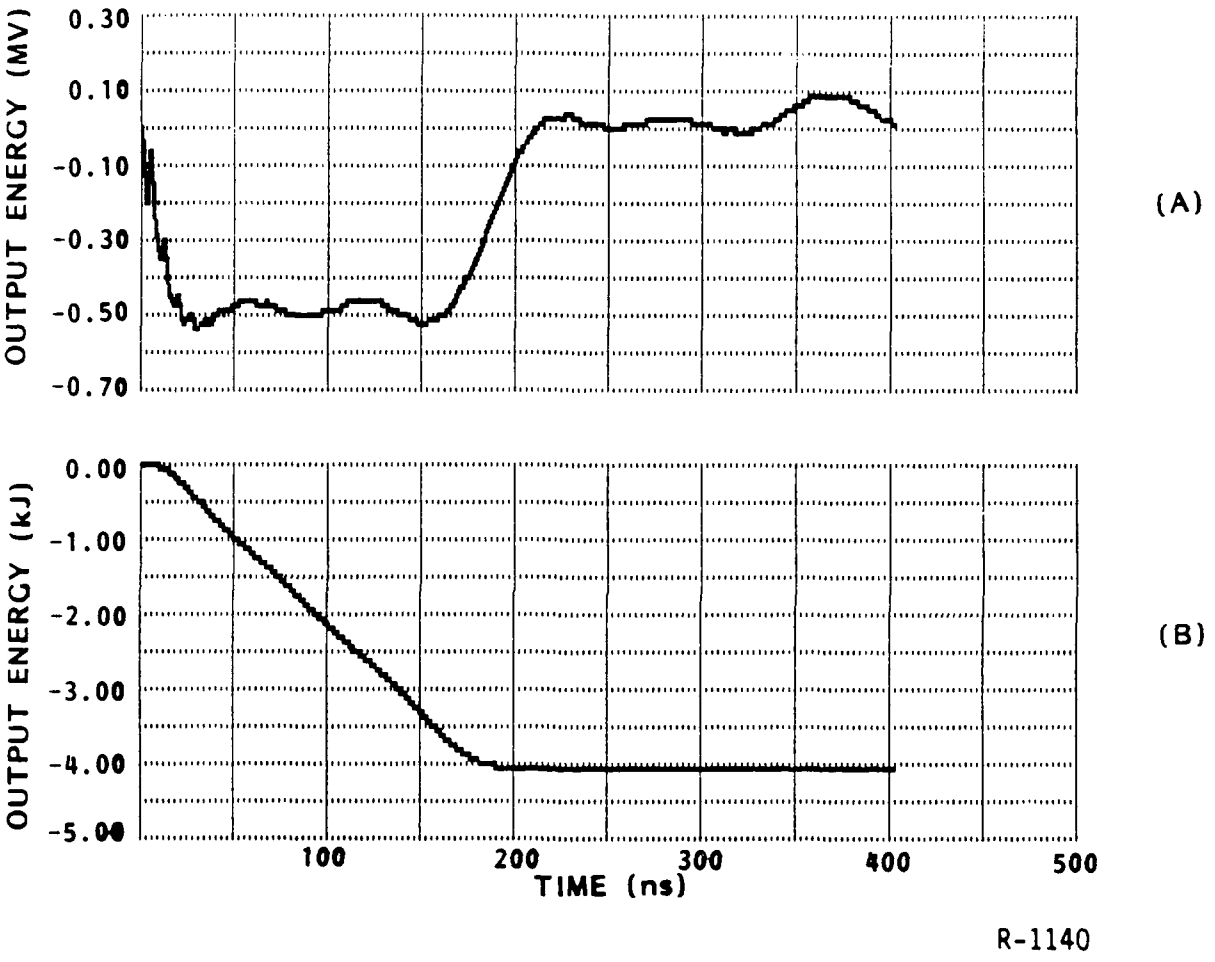

Figure 23. Output voltage (A) and output energy (B) of 10 Ω, 150 ns, 4 kJ PFN.

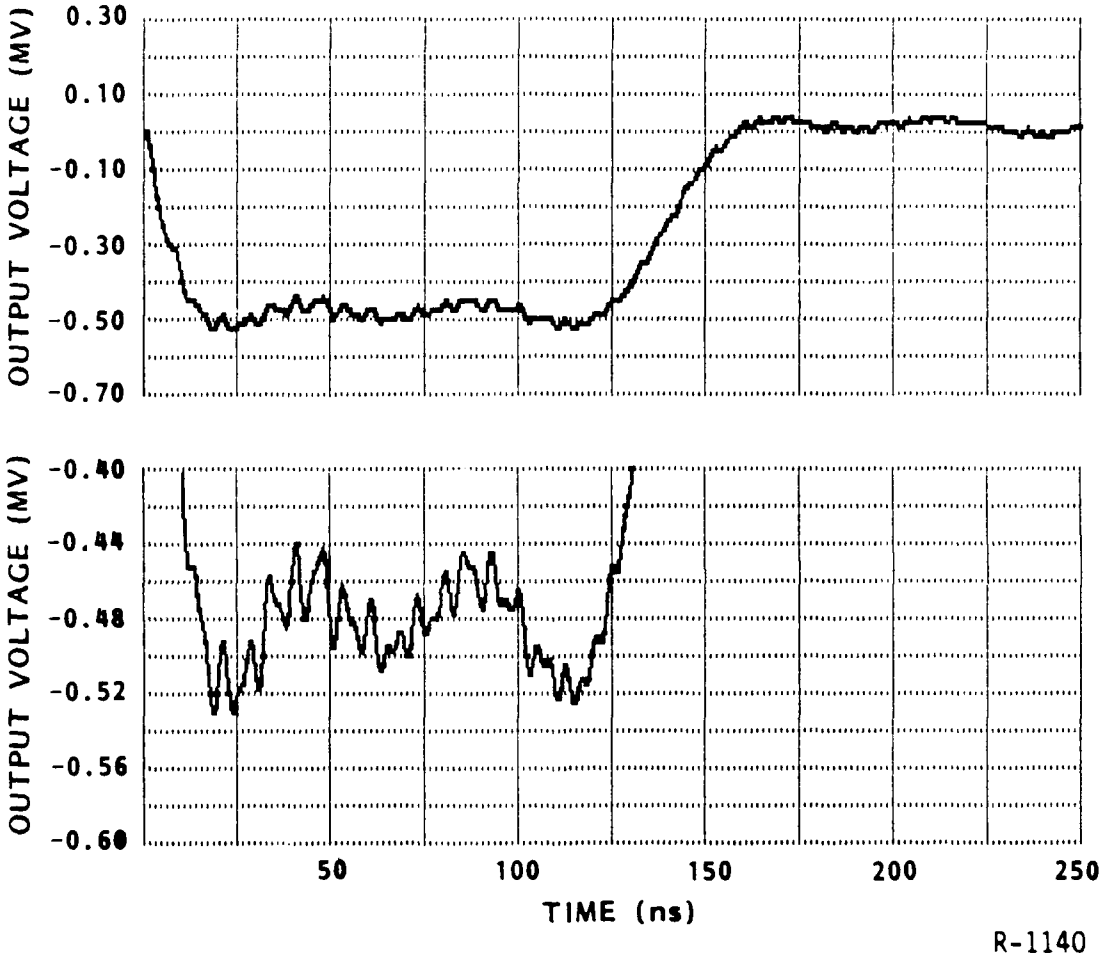

Figure 24. Output voltage of 10 Ω, 100 ns, 3 kJ PFN with 25 nH and 106 nH inductors of Figure 18 interchanged. (A) full scale, (B) smaller voltage scale.

dielectric. Finally, the dielectric constant of water can be varied by the addition of ethylene glycol (Ref. 12). As described above, this variation of in dielectric constant allows variation in the output performance of the pulser.

Unfortunately, water has a limited temperature range. The addition of the ethylene glycol can extend this range to a maximum spread of temperatures from -45° C to +110° C. However, the dielectric constants of these water and glycol mixtures are also temperature dependent. Figure 25 shows the dielectric constant of water and glycol mixtures for various temperatures and percentages of glycol by weight. The end points to the left of the curves represent the freezing points of the mixtures. Temperature effect were simulated for the 10 Ω, 100 ns pulser design with a 40:60 water:glycol mixture. The results are shown in Figure 26 for -45° C, +30° C, and +110° C.

At lower temperatures the output pulses were lower in amplitude and longer in pulse width while higher temperatures produced higher voltages and shorter pulse widths. At the lower temperatures, the capacitors of the PFN had higher capacitances in accordance with Figure 25. Consequently, the capacitors were unable to achieve full 1 MV charges. Longer pulse lengths at lower voltages were the result of higher PFN capacitances. From Equation 4 the pulse width and PFN capacitances are directly proportional. Thus, higher capacitances yield longer pulse lengths. The effects at higher temperatures were the results of the same mechanisms that occurred at lower temperatures but with opposite trends.

Extensive electric field simulations of the PFN components were conducted. These simulations were performed to insure that no field values exceeded limits in the different media of the PFN. An equipotential plot of a JASON calculation for the capacitor C_3 is shown in Figure 27. Figure 28 shows the equipotentials for the inductor region of L_5. The diamond shapes in the lower portions of the figure are JASON's representation of the inductor conductors. The equipotentials at the peak voltage of the charging cycle are shown in Figure 28(a). After the output switch closes, the voltages between elements of the PFN obviously change with time. At 93 ns after switch closure, the maximum voltage is impressed across L_5 and the equipotentials at this time are shown in Figure 28(b). A voltage difference of 440 kV across L_5 occurs at 93 ns with the left conductor (C_5) at -865 kV and the right conductor (C_3) at -425 kV. Table 4 lists the maximum field strengths at different locations in the PFN (shown in Figure 29) as calculated by JASON and the maximum allowable field strengths in the media at those locations.

Typically, insulator surfaces have the lowest breakdown field strengths of any components within pulsed power machines. Breakdown occurs along the surfaces of such insulators or interfaces (referred to as surface flashover) no matter what medium the

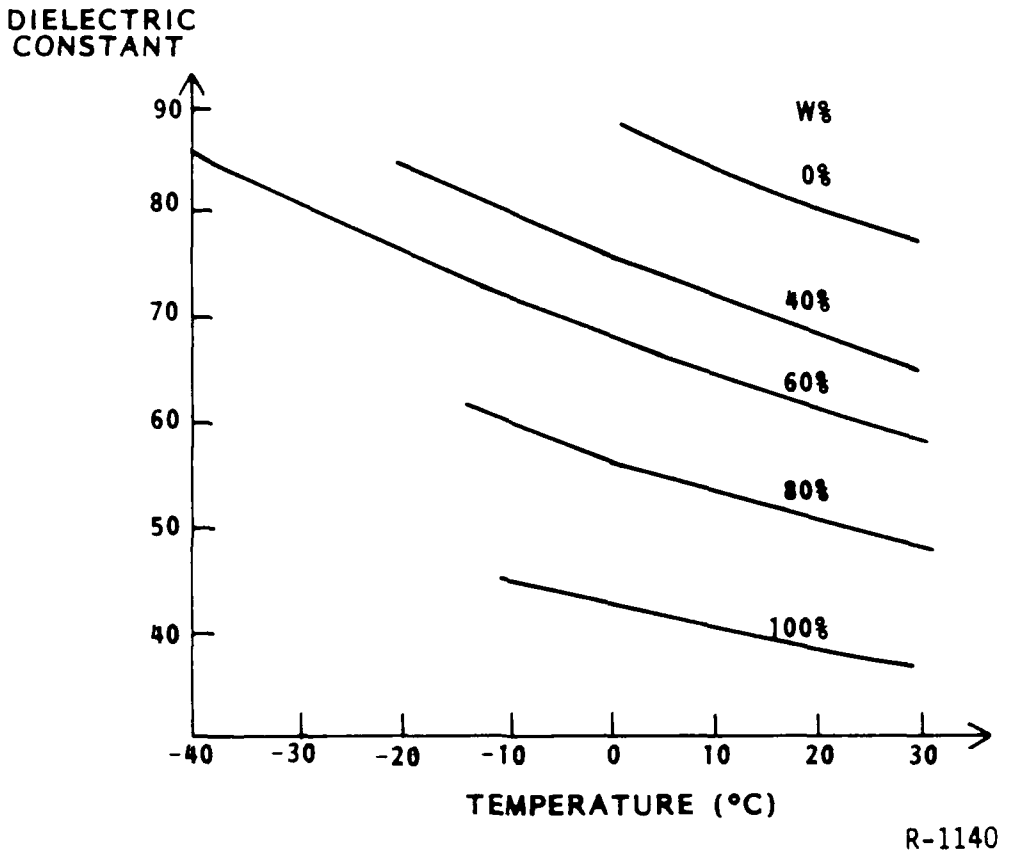

Figure 25. Temperature dependence of the dielectric constant of water and ethylene glycol mixtures. W is the percent by weight of ethylene glycol. Lower temperature end points of the curves are the freezing points of the mixtures.

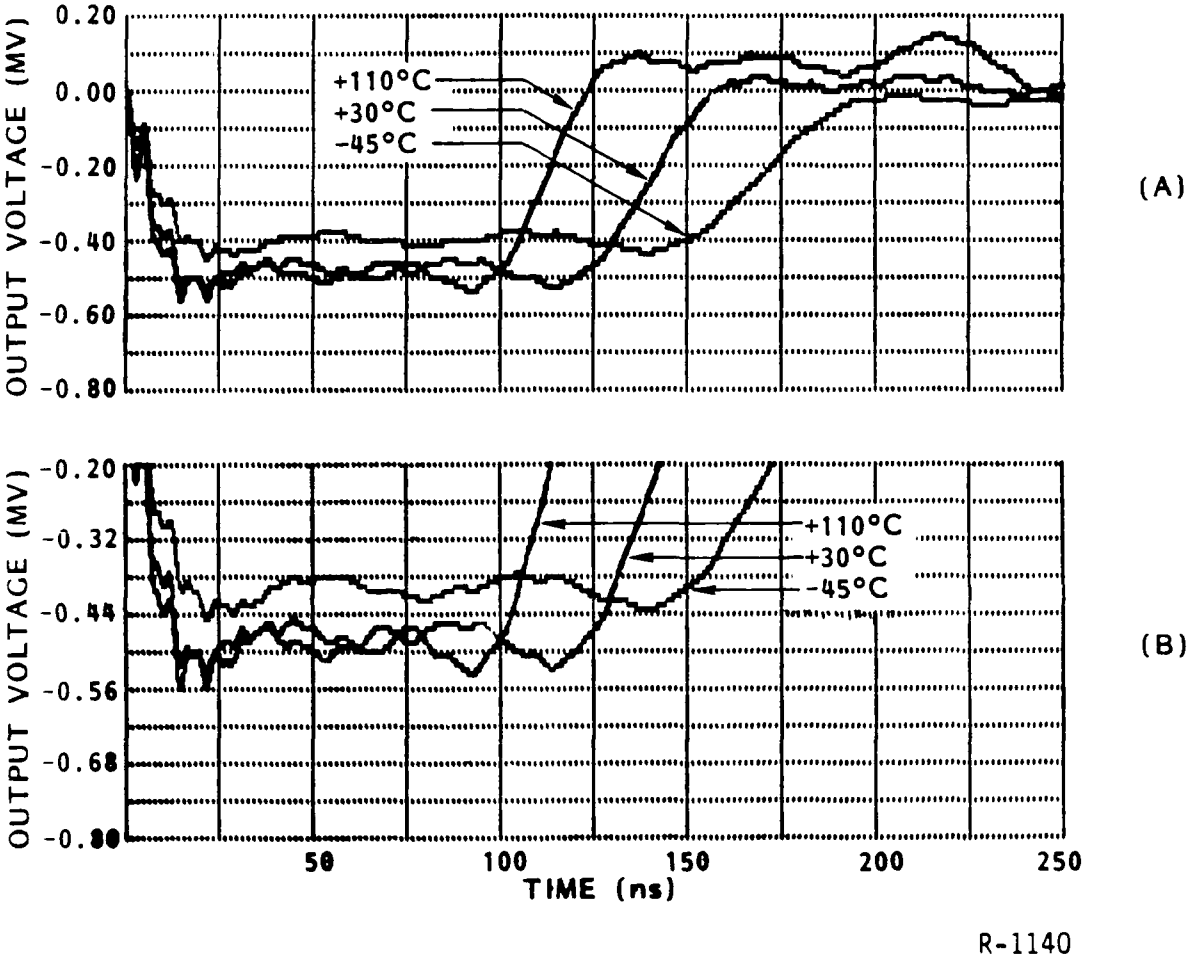

Figure 26. Output voltage of 10 Ω, 100 ns, 3 kJ PFN under varying temperatures, (A) full scale, (B) smaller voltage scale.

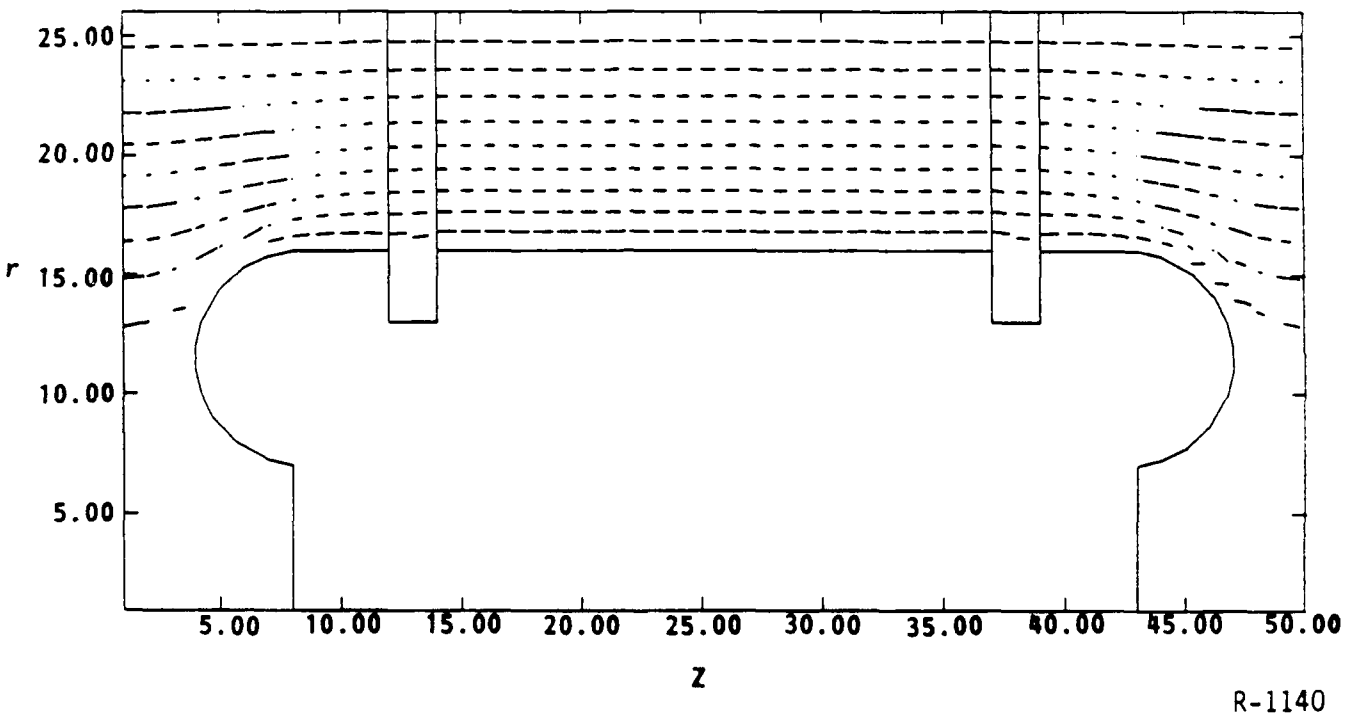

Figure 27. Equipotential field lines of the second PFN capacitor (C_3). 100 kV separates each line. Dimensions shown are in cm.

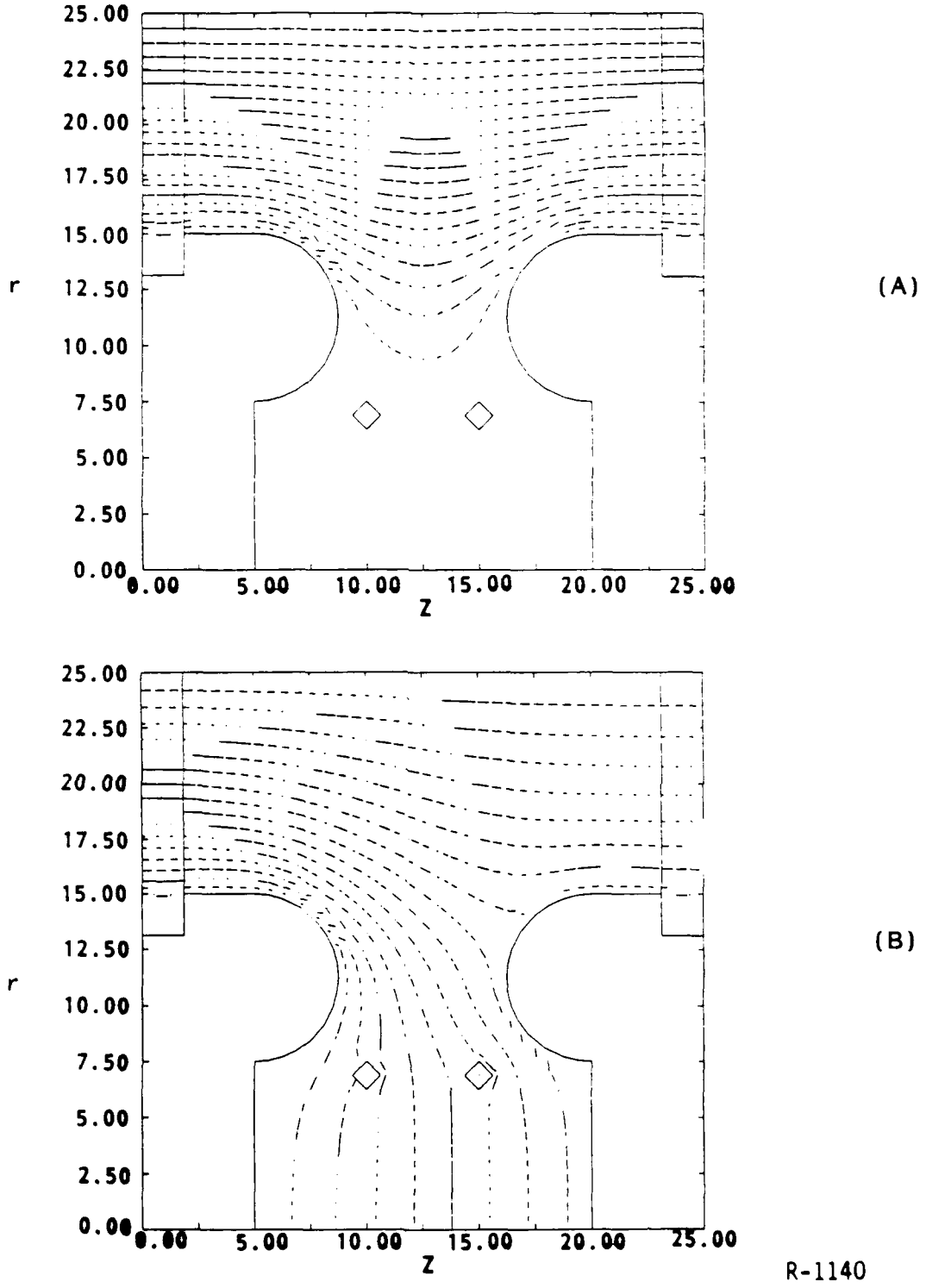

Figure 28. Equipotentials of gas filled region of inductor L_5, (A) at peak voltage of charging cycle (1 MV), and (B) 93 ns after output switch closure. The diamonds in lower portion of figures are sections of the inductor coil. Dimensions are in cm.

TABLE 4. Maximum electric field strengths.

Location in Figure 29	Charging/Discharging	Electric Field Strength (kV/cm)	Breakdown Field Strength (kV/cm)
Ⓐ	Charging	400	400
Ⓑ	Charging	243	400
Ⓒ	Charging	151	400
Ⓓ	Charging	162	250
Ⓔ	Charging	130	250
Ⓕ	Charging	143	187
Ⓖ	Charging	184	250
Ⓗ	Charging	154	250
Ⓘ	Charging	130	187
Ⓐ	Discharging	0	400
Ⓑ	Discharging	118	400
Ⓒ	Discharging	136	400
Ⓓ	Discharging	216	250
Ⓔ	Discharging	141	250
Ⓕ	Discharging	143	187
Ⓖ	Discharging	170	250
Ⓗ	Discharging	131	250
Ⓘ	Discharging	130	187

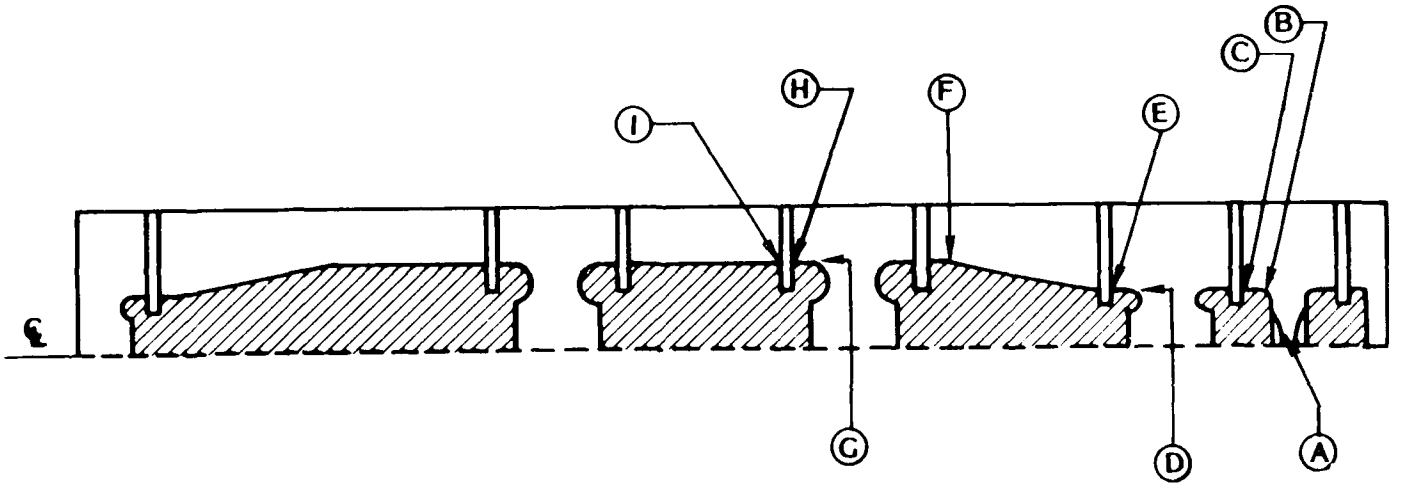

Figure 29. Locations of maximum electric fields in PFN.

insulator may be in. For the gas side of the insulators of the PFN, the gas pressure can be increased to prevent surface flashover (Refs. 19, 20,and 21). However, the electric fields on the water side of the insulators must be carefully controlled to avoid flashover. The flashover strengths can be made equal to the breakdown strength that the dielectric is immersed in by insuring that the electric field vectors along the surface are parallel to the surface (Ref. 17, 22). JASON was utilized to design field shaping structures near the insulators to reduce the electric field vector components directed into the insulator surfaces. The toroidal shaped structures at the ends of the capacitors are the resulting field shaping structures.

The PFN inductors were designed as described in Chapter 3. The dimensions of the coils were calculated using Equation 18 and Grover's (Ref. 14) algorithms. The lengths and radii of the coils were adjusted to minimize the electric field strengths resulting from the voltage between the coils and the surrounding structures and between turns of the coils. Thus the radii were adjusted to minimize the electric field between the coil and the outer conductor at peak charge voltage according to Equation 16. JASON calculations for this case are shown in Figure 28(a). The coil spacing (i.e., the pitch) was adjusted to prevent breakdown from one turn to the next. The appropriate spacing was confirmed by JASON simulations as shown in Figure 28(b). The coil conductor diameter (1 cm) was chosen to reduce the field enhancement factor. The only remaining free variable allowed to adjust the inductance was the number of turns. Table 5 lists the number of turns necessary for the different inductors and for different impedance/pulse width parameters.

The output switch design utilizes a high voltage spark gap operated under self-breakdown conditions. The switch pressure is adjusted so that the spark gap closes at the peak of the charge voltage. The electrode design incorporates inserts composed of copper-tungsten composites in order to reduce electrode erosion. The design allows gas flow through the spark gap for repetitive operations. The amount of flow is difficult to calculate and would have to be determined empirically from a prototype pulser. However, Buttram (Ref. 23) has suggested that no gas flow may be necessary at the repetition rates considered for this design (10 Hz). An alternative switch design is shown in Figure 30. This alternative design forces breakdown in an annular area away from the pulser axis. In this way, arc damage is spread over a larger are with a consequential reduction in electrode erosion. The gas is injected into the spark gap on axis and flows over the surface of the cathode and the insulator region nearest the cathode. This gas flow cools the electrode surface (which allows lower gas flow) and removes breakdown particulate matter from collecting on the insulator (Ref. 24).

Unlike laboratory pulsers, the pulsers in this report have been designed to operate over temperature ranges as large as are possible. The maximum and minimum service

TABLE 5. Inductor parameters.

(length = 15 cm, radius = 7 cm)

n	k_n	z = 10 Ω		z = 20 Ω		z = 50 Ω	
		L_n (nH)	N_n	L_n (nH)	N_n	L_n (μH)	N_n
1	.1185	166	1.35	664	2.70	4.15	6.75
3	.1060	150	1.28	600	2.57	3.74	6.41
5	.1427	200	1.48	800	2.97	5.00	7.42
Pulse Length		100 ns		200 ns		500 ns	

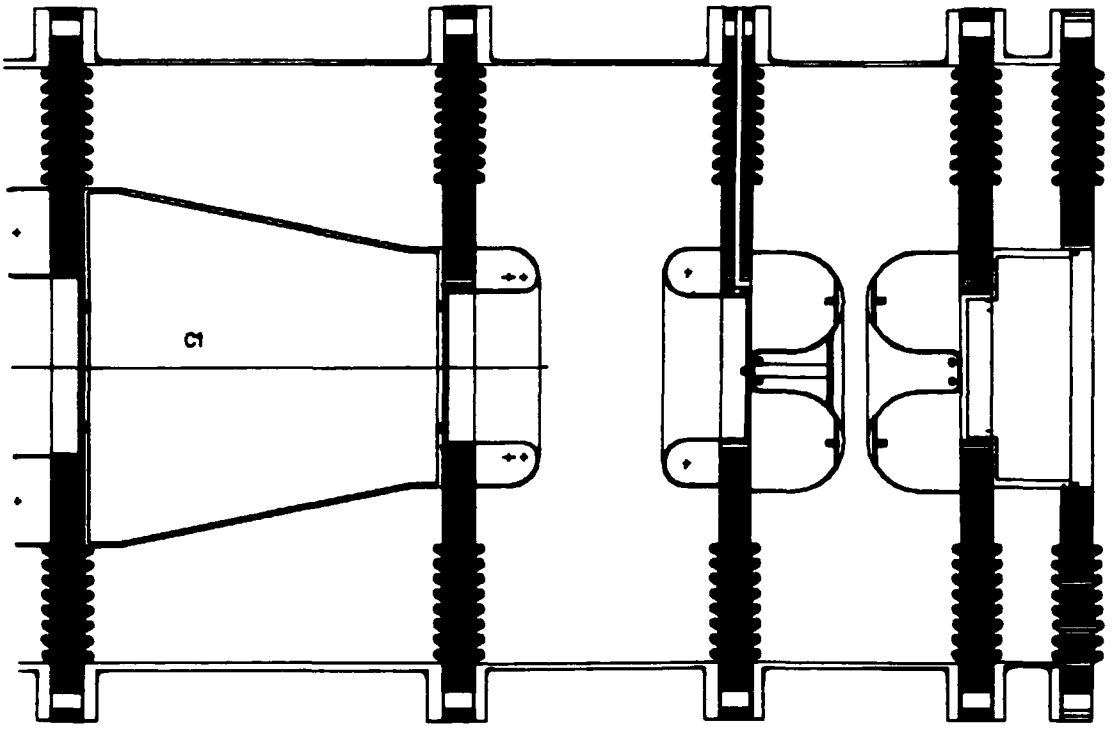

Figure 30. Alternative output switch design.

temperatures of materials that would be used in the pulsers are listed in Table 6. The upper limit corresponds to the boiling point of the water and ethylene glycol mixture of the PFN capacitors. Somewhat higher boiling points may actually occur since the high voltage sections of the pulsers would be pressurized during operations. Transformer oil for the transformer limits the lower operating point. Replacing transformer oil with a gas insulator (SF_6 or fluorocarbons) would lower the lower operating temperature (-45° C) and reduce weight. Insulators fabricated from alumina filled conventional epoxies would allow insulators with thermal expansion coefficients equal to that of aluminum. Cycloaliphatic epoxies also filled with alumina have been proposed for stand-offs in high voltage, gas insulated power transmission cables.

Associated with the issue of temperature tolerance is the issue of waste heat management. Under the worst conditions, however, the thermal mass of the pulser may be used to absorb the heat for short bursts of operations. For example, suppose that all of the energy of the 3 kJ design is to be absorbed by only the water of the capacitors and that a 50° C increase in temperature is allowed. Then the pulser could operate at 10 Hz for approximately 15 minutes. Obviously, the mass of the structural components of the pulser and a somewhat efficient load would allow longer operating times.

4.3 Transformer and Primary Circuit Design

The PFN would be charged, through a step-up transformer, by a bank of lower voltage capacitors. The transformer design is of the spiral strip type with a single turn primary and multiple secondary turns inside of the primary turn. Essentially, the secondary windings are stacked radially with the high voltage output at the inner most winding and is led out through the center of the assembly by a rod on axis. This design is much less prone to breakdown as a result of the stacked winding arrangement (Refs. 25, 26). Fast rising voltage pulses are capacitively graded by the stacked capacitances of the secondary windings. However, structures must be designed to shape the electric fields at the edges of the wide, flat windings. Otherwise, breakdown will occur from winding to winding at the winding edges.

The transformer would be operated in dual resonance. One performance parameter of a transformer is its coupling coefficient (k) which is given by,

$$k = \frac{M}{\sqrt{L_1 L_2}} \quad , \tag{21}$$

TABLE 6. Material thermal properties.

MATERIAL	SERVICE TEMPERATURE RANGE	COEFFICIENT OF THERMAL EXPANSION
Water/Ethylene Glycol (40%/60%)	-51°C to +112°C	–
Transformer Oil	-45°C to +135°C	–
Sulfur Hexafluoride	-64°C to +330°C	–
Epoxy (Cycloaliphatic)	to +230°C	2.4 to 5.4 $\times 10^{-5}$/°C
Aluminum	–	2.3 to 2.4 $\times 10^{-5}$/°C
TOTAL SYSTEM	-45°C to +112°C	

VG-0959

where L_1 is the total inductance of the primary circuit of the transformer, L_2 is the secondary circuit inductance, and M is the mutual inductance between the windings of the transformer. Now, if a capacitor, C_2, on the secondary side of a transformer is charged by a capacitor, C_1, on the primary side with an initial voltage, V_o, the secondary voltage, $v_{C2}(t)$, may be expressed by (Ref. 27):

$$v_{c2}(t) = \frac{V_o}{2} \left(\frac{L_2}{L_1}\right)^{1/2} \left[\cos \frac{\omega t}{\sqrt{1-k}} - \cos \frac{\omega t}{\sqrt{1+k}}\right] \quad . \tag{22}$$

This is illustrated in Figure 31. For the capacitor C_2 to be charged within the first half-cycle of the two cosine terms, the coupling coefficient, k, must be as large as possible (i.e., $k = 1$). If k is not large, only low energy transfer efficiencies are obtained.

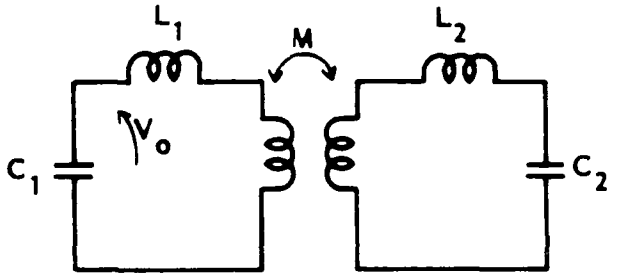

R-1140

Figure 31. Transformer charging of a capacitor.

Unfortunately, coupling coefficients higher than about 0.85 are not possible in practice. An alternative is to allow the peak voltage on C_2 to occur on the second-half cycle. Such operations are referred to as dual resonance. For dual resonance, a theoretical maximum energy transfer of 100% is achieved on the second and negative half cycle. The coupling coefficient must be 0.6 (which may be constructed easily) and the frequency of operation must follow:

$$L_1 C_1 = L_2 C_2 = \frac{1}{\omega^2} \quad . \tag{23}$$

Dual resonance transformers of the spiral type have successfully charged pulse-forming lines to 3 MV with 90% efficiency and under repetitive pulse applications (Refs. 25,

and 26). For the 3 kJ pulser, a coupling coefficient of 0.6 could be achieved with the inductor values of $L_1 = 1.02\ \mu H$, $L_2 = 310\ \mu H$, and $M = 13\ \mu H$. Figure 32 shows the charging waveforms for the 10 Ω, 100 ns PFN design with the above inductor values. The primary capacitor bank capacitance was 1.22 μF charged to 70 kV. Three Maxwell Type SS capacitors form the primary capacitor bank and are shown in Figure 16. For the different PFN energy designs (i.e., the 4 kJ versus the 3 kJ design), different size primary capacitor banks are necessary. This requirement is a consequence of dual resonance which, by its name, requires:

$$\omega = \frac{1}{\sqrt{L_1 C_1}} = \frac{1}{\sqrt{L_2 C_2}} \quad , \tag{24}$$

as well as energy conservation.

Additionally, the larger C_1 and C_2 values will increase the charging time for the PFN.

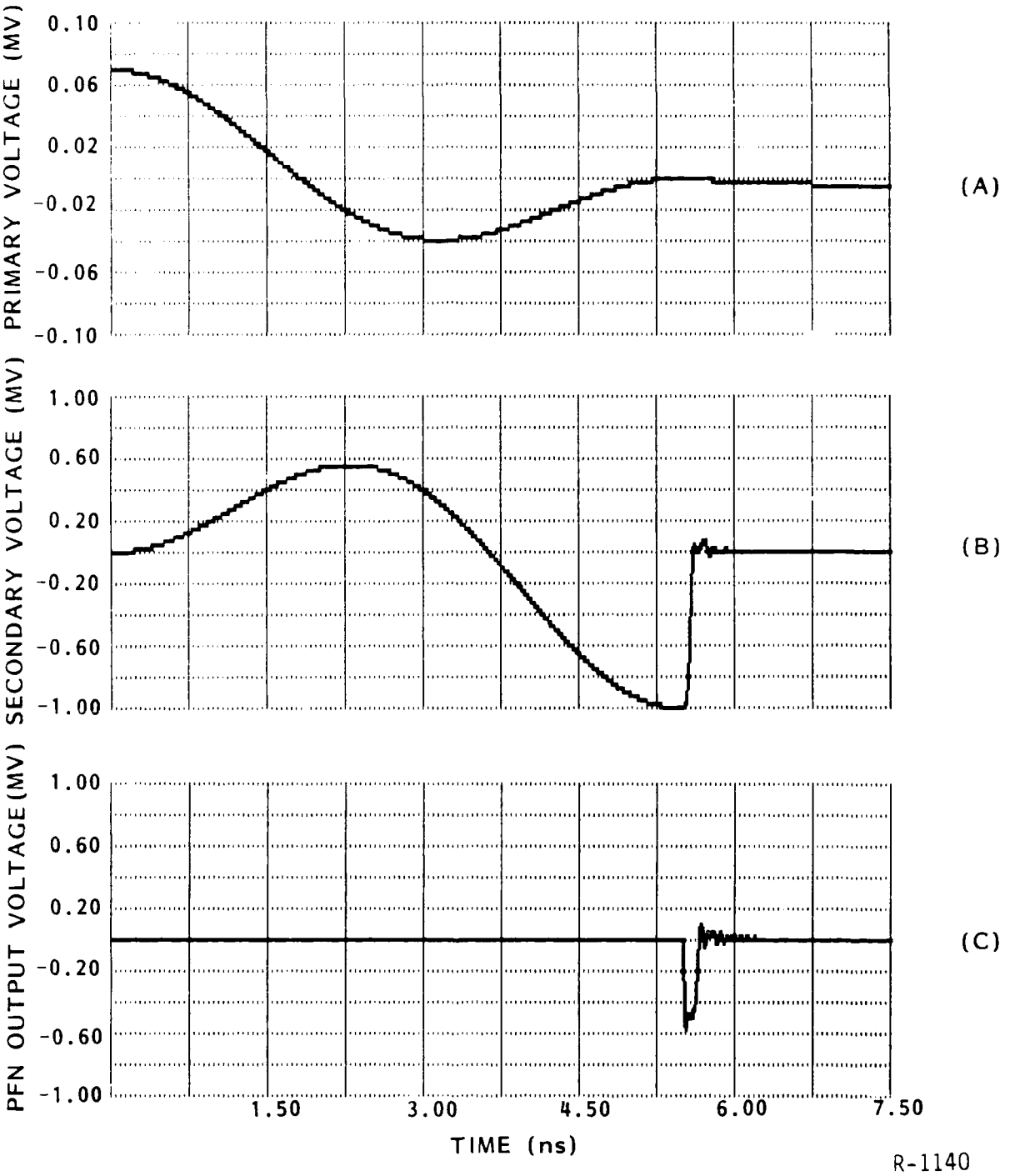

Figure 32. Transformer voltages: (A) primary, (B) secondary, and (C) PFN output.

5.0 CONCLUSION

The Phase I design study essentially produced two designs for a compact, repetitively pulsed, -500 kV pulsed power sources. The first design is capable of low energies (800 J) into high impedance loads (100 Ω) and fast rise times (1 ns). The low energy design exceeds the original design goals as outlined in the introduction. The second design is capable of producing 3 to 4 kJ outputs into loads of from 10 to 50 Ω and pulse widths from 100 to 500 ns. This design allows great flexibility in mechanically "tuning" the pulser to specific load impedances and output pulse widths. A pulser built from the second design would be contained in a volume measuring 2 ft in diameter and 10.9 ft long and would weigh 1,300 lbs. Thus the second design meets the volume goals and comes close to the weight goals of the design study despite a six fold increase in the energy goal. Production costs for the 3–4 kJ design could be lower than $15,000 per copy.

6.0 ACKNOWLEDGEMENTS

The author would like to thank Gary Estepp, Gary Hess, Cliff Woods, and Don Sullivan (all of MRC) and Gerry Rohwein (of Sandia National Laboratories) for their technical suggestions and assistance.

REFERENCES

1. "Airborne/Spaceborne Pulsed Power Source," Mission Research Corporation, MRC Proposal No. P8132.02, Albuquerque, NM, p. 3, 1988.

2. White, H. J., P. R. Gillette, and J. V. Lebacqz, "The Pulse-Forming Network," in *Pulse Generator*, ed. G. N. Glascoe and J. V. Lebacqz, (McGraw-Hill Book Co., New York), p. 175, 1948.

3. Butcher, R., "Transmission Lines and Pulse Forming Networks," in *Pulse Power Lecture Series*, ed. M. Kristiansen and A. H. Guenther, supported under AFOSR Grant No. 78-3675, Texas Tech University, p. 16.

4. Hess, G., Mission Research Corporation, private communication, 1987.

5. Pohl, H. A., "Superdielectrics Polymers," *IEEE Trans. on Elect. Insulation*, EI-21, p. 683, 1986.

6. Guillemin, E. A., "A Historical Account of the Development of a Design Procedure for Pulse-Forming Networks," Radiation Laboratory Report No. 43, p. 1, 1944.

7. Krompholz, H., J. R. Cooper, J. Doggett, K. H. Schoenbach, and G. Schaefer, "Slow Wave Line-Type Pulsers," in *Conf. Record 1986 Seventeenth Power Modulator Symposium*, Seattle, WA, p. 207, 1986.

8. Watkins, D. A., *Topics in Electromagnetic Theory*, (John Wiley and Sons, New York), p. 1, 1958.

9. van Valkenburg, M. E., *Introduction to Modern Network Synthesis*, John Wiley and Sons, New York, p. 128, 1960.

10. Sackett, S. J., JASON—A Code for Solving General Electrostatic Problems: User's Manual, Lawrence Livermore Laboratory, p. 1, 1978.

11. Hayt, W. H., *Engineering Electromagnetics*, (McGraw-Hill Book Co., New York), p. 407, 1974.

12. Fenneman, D. B., and R. J. Gripshover, "High Power Dielectric Properties of Water Mixtures," in *Proc. Fourth IEEE Pulsed Power Conf.*, Albuquerque, NM, p. 302, 1983.

13. Martin, J. C., "Nanosecond Pulse Technique," 1970.

REFERENCES (CONTINUED)

14. Grover, F. W., Inductance Calculations, Instrument Society of America, Research Triangle Park, NC, p. 142.

15. Fenneman, D. B., and R. J. Gripshover, "Experiments on Electrical Breakdown in Water in the Microsecond Regime," *IEEE Trans. Plasma Sci.*, PS-8, p. 209, 1980.

16. Sincerny, P. S., "Electrical Breakdown Properties of Water for Repetitively Pulsed Burst Conditions," in *Proc. Fifth IEEE Pulsed Power Conf.*, Arlington, VA, p. 222, 1985.

17. Etlicher, B., N. Camarcat, C. Bruno, G. Raboisson, and A. Perronnet, "Scaling of the J. C. Martin Breakdown Equations to Generators of the 1-TW Class," in *Proc. Fourth IEEE Pulsed Power Conf.*, Albuquerque, NM, p. 331, 1983.

18. Rohwein, G. J., "Partial Discharge Formation and Breakdown in Deionized Water Under Repetitive Stressing," in *Proc. Fifth IEEE Pulsed Power Conf.*, Arlington, VA, p. 339, 1985.

19. Laghari, J. R., and A. H. Qureshi, "Surface Flashover of Spacers in Compressed Gas Insulated Systems," *IEEE Trans. on Elect. Insulation*, EI-16, p. 373, 1981.

20. Sudarshan, T. S and R. A. Dougal, "Mechanisms of Surface Flashover Along Solid Dielec s in Compressed Gases: A Review," *IEEE Trans. on Elect. Insulation*, EI-21, p. 727, 1986.

21. Cookso, A. H., "Insulators in Compressed Gas," *IEEE Proc.*, 128, p. 303, 1981.

22. Miller, A. R., "Sub-Ohm Coaxial Pulse Generators, Blackjack 3, 4, and 5," in *Proc. Third IEEE Pulsed Power Conf.*, Albuquerque, NM, p. 200, 1981.

23. Buttram, M., "An Alternative to Gas Purging in Pulse Charged Repetitive Spark Gaps," in *Proc. Fourth IEEE Pulsed Power Conf.*, Albuquerque, NM, p. 163, 1983.

24. Rohwein, G. J., Sandia National Laboratories, private communication, 1988.

25. Rohwein, G. J., "Pulse Transformers and Dielectrics," in *High Voltage/Pulse Power Technology and Power Conditioning Technology Lecture Notes*, ed. W. Sarjeant, University of New Mexico and Los Alamos National Laboratories, Albuquerque, NM, Lecture No. 9, 1980.

REFERENCES (CONCLUDED)

26. Sarjeant, W. J., and G. J. Rohwein, "A Review of Repetitive Pulse Power Component Technology," in *Proc. Fourth IEEE Pulsed Power Conf.*, Albuquerque, NM, p. 631, 1983.

27. Cook, E., and L. Reginato, "Off-Resonance Transformer Charging for 250-kV Water Blumlein," in *Conf. Record 1978 Thirteenth Pulse Power Modulator Symposium*, Buffalo, NY, p. 27, 1978.

APPENDIX A
MACHINE DRAWINGS FOR 3-4 KJ PULSED POWER SOURCE

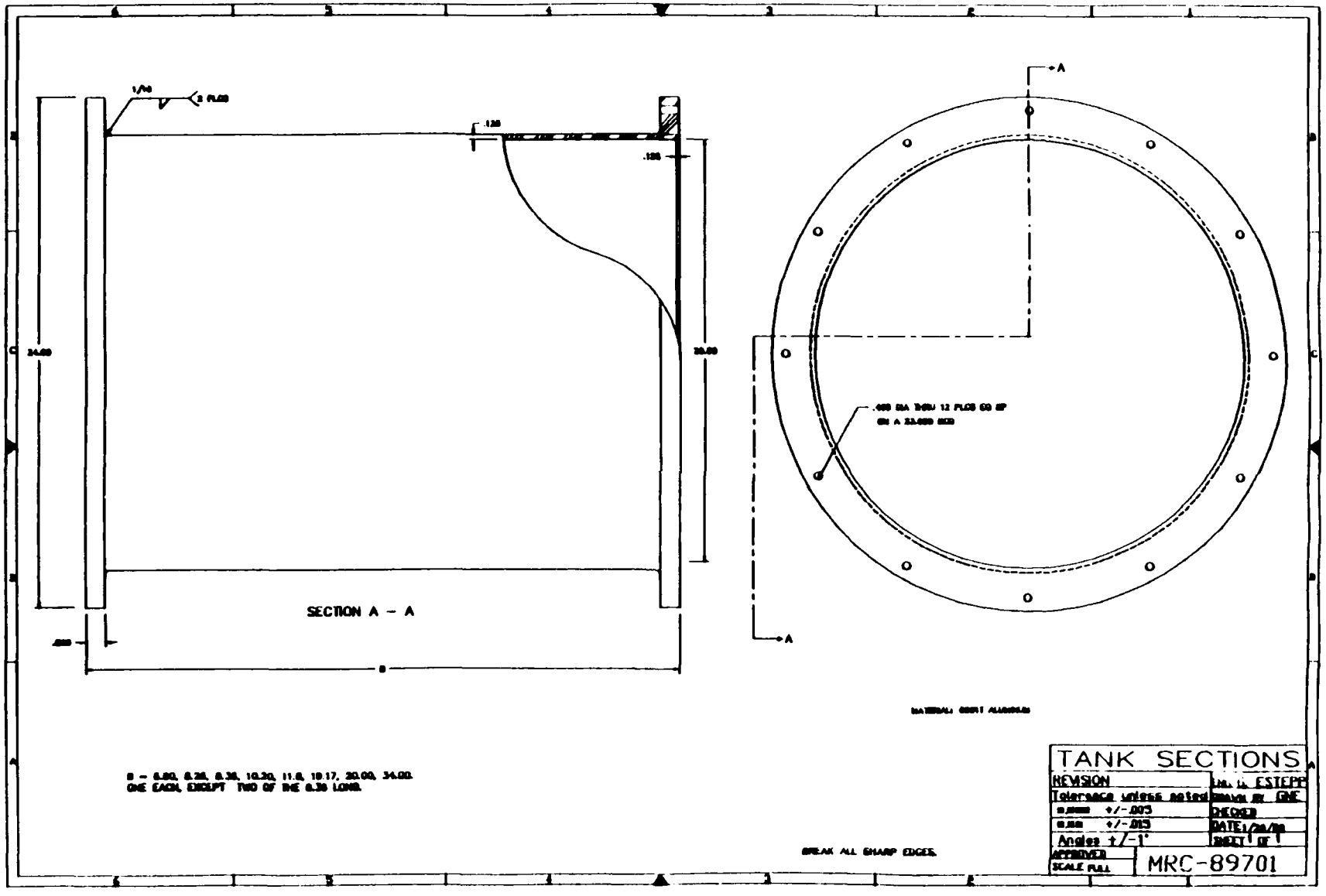
SECTION A – A
A
A
8 – 6.80, 8.26, 8.36, 10.30, 11.8, 19.17, 20.00, 34.00
ONE EACH, EXCEPT TWO OF THE 8.36 LONG.
BREAK ALL SHARP EDGES.
TANK SECTIONS
REVISION
Tolerance unless noted
+/-.005
+/-.015
Angles +/-1°
APPROVED
SCALE FULL
MRC-89701

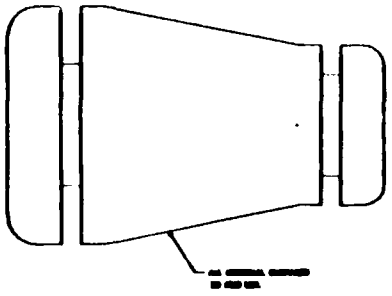

ASSEMBLY

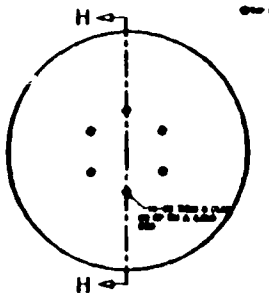

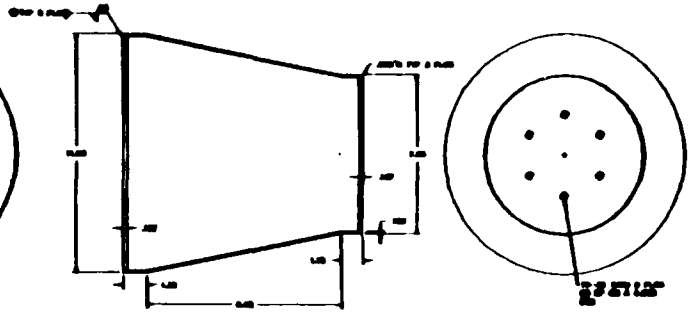

SECTION H - H

PART -03

MATERIAL: 6061 O ALUMINUM
BREAK ALL SHARP EDGES.
SURFACE FINISH TO 32 RMS

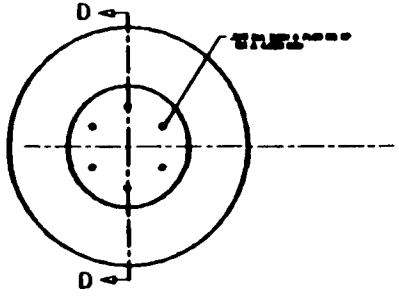

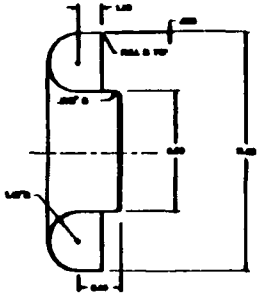

SECTION D - D

PART -01

MATERIAL: 6061 O ALUMINUM
BREAK ALL SHARP EDGES.
SURFACE FINISH TO 32 RMS

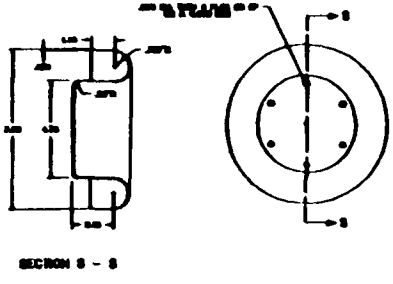

PART -02

MATERIAL: 6061 O ALUMINUM
BREAK ALL SHARP EDGES.
SURFACE FINISH TO 32 RMS

C1 PARTS	
REVISION	DR. G. ESTEPP
Tolerance unless noted	DRAWN BY GNE
.xxx +/-.005	CHECKED
.xx +/-.015	DATE 2/1/00
Angles +/-1°	SHEET 1 OF 1
APPROVED	MRC-89702
SCALE FULL	

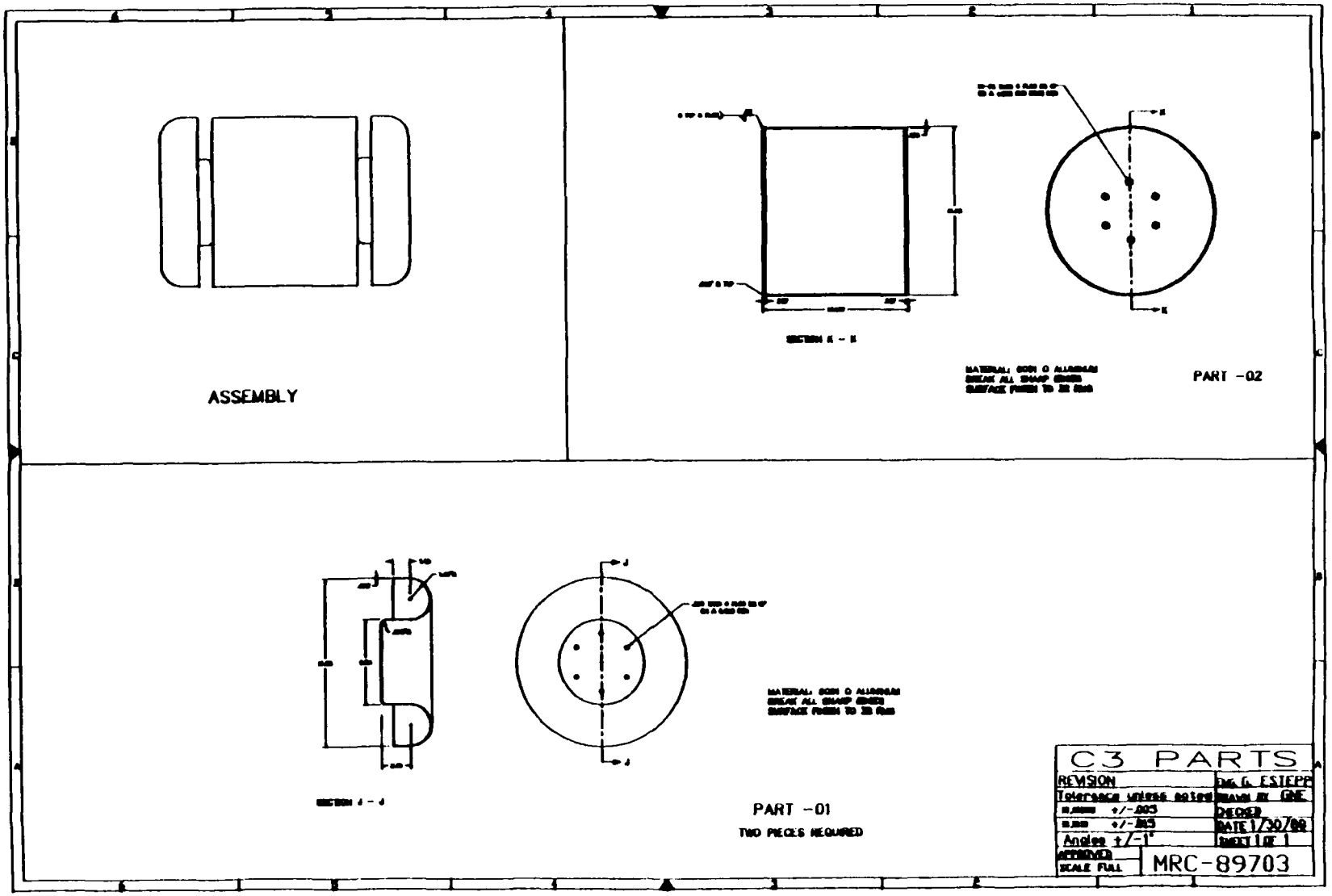
ASSEMBLY
PART -02
PART -01
TWO PIECES REQUIRED
C3 PARTS
REVISION
Tolerance unless noted
+/-.005
+/-.015
Angles +/-1°
APPROVED
SCALE FULL
DWG G. ESTEPP
DRAWN BY GNE
CHECKED
DATE 1/30/08
SHEET 1 OF 1
MRC-89703

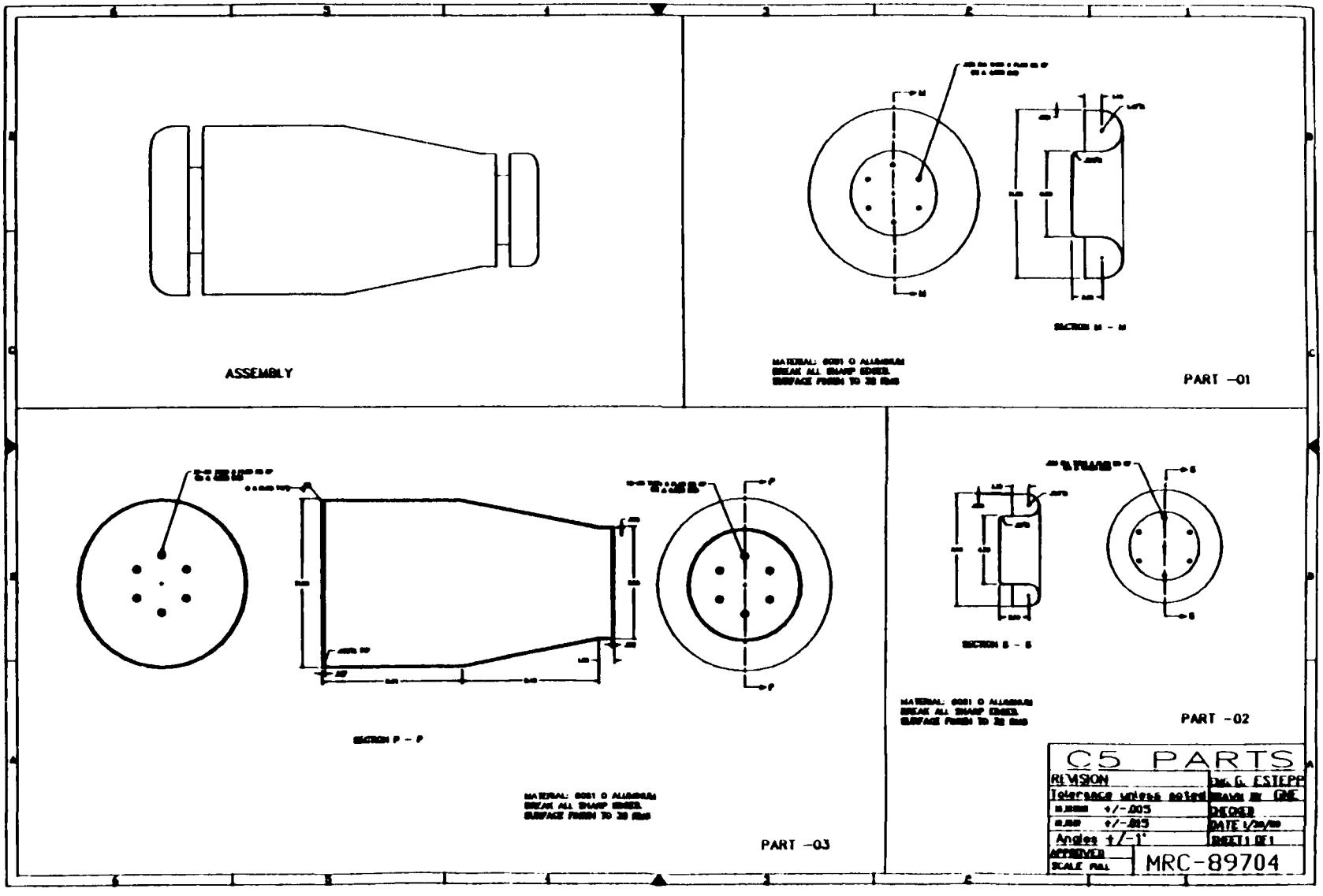
ASSEMBLY
PART -01
PART -02
PART -03
C5 PARTS
REVISION
Tolerance unless noted
+/-.005
+/-.005
Angles +/-1°
APPROVED
SCALE FULL
MRC-89704
DRAWN BY G. ESTEPP
CHECKED
DATE 1/20/00
SHEET 1 OF 1

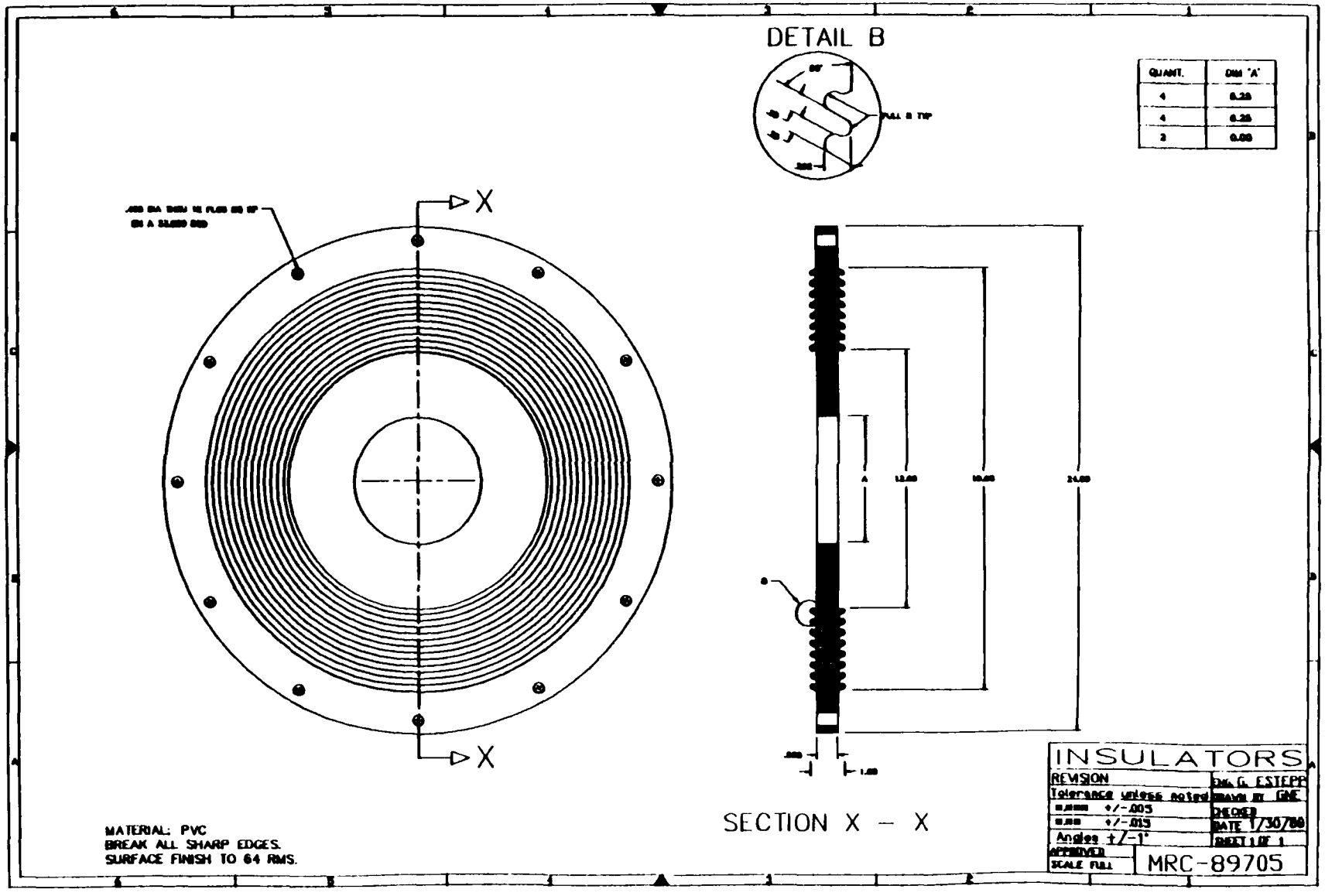
DETAIL B
QUANT.
DIM 'A'
X
X
SECTION X – X
MATERIAL: PVC
BREAK ALL SHARP EDGES.
SURFACE FINISH TO 64 RMS.
INSULATORS
REVISION
Tolerance unless noted
.xxxx +/-.005
.xxx +/-.015
Angles +/-1°
APPROVED
SCALE FULL
DWG. G. ESTEPP
DRAWN BY GME
CHECKED
DATE 1/30/80
SHEET 1 OF 1
MRC-89705

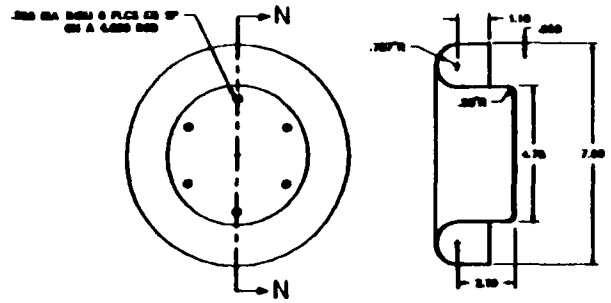

SECTION N – N

BREAK ALL SHARP EDGES.
SURFACE FINISH TO 32 RMS.

MATERIAL: 6061 O ALUMINUM

PART –01

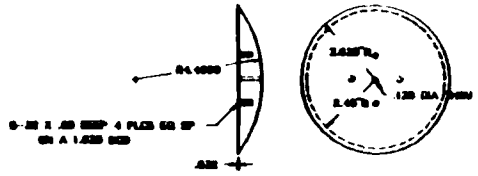

TUNGSTEN–COPPER
(OR ALCONITE)

TWO PIECES REQUIRED

BREAK ALL SHARP EDGES.

PART –03

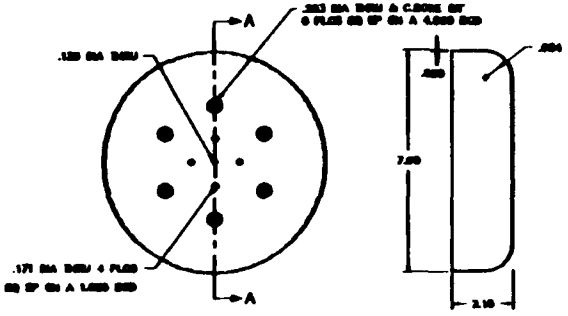

TWO PIECES REQUIRED

MATERIAL: 6061 O ALUMINUM

SECTION A – A

BREAK ALL SHARP EDGES.
SURFACE FINISH TO 32 RMS.

PART 02

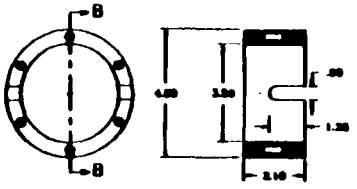

SECTION B – B

BREAK ALL SHARP EDGES.
SURFACE FINISH TO 32 RMS.

MATERIAL: 6061 O ALUMINUM

TWO PIECES REQUIRED

PART –04

SWITCH PARTS	
REVISION	ENG G. ESTEPP
Tolerance unless noted	DRAWN BY GNE
.xxx +/-.005	CHECKED
.xx +/-.015	DATE 2/1/88
Angles +/-1°	SHEET 1 OF 1
APPROVED	MRC-89706
SCALE FULL	

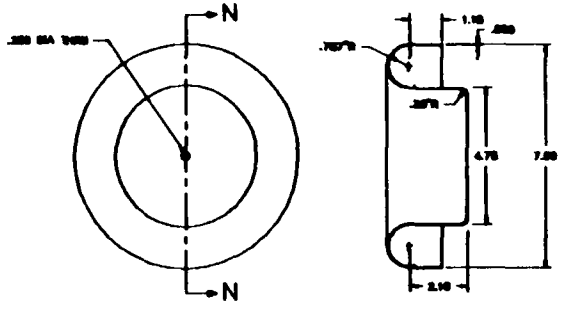

SECTION N – N

BREAK ALL SHARP EDGES.
SURFACE FINISH TO 32 RMS.

MATERIAL: 6061 O ALUMINUM

PART –01

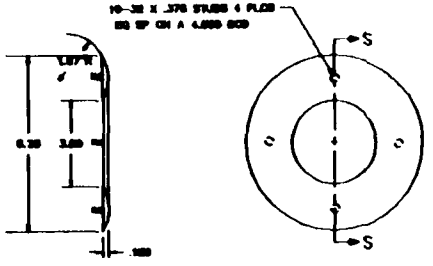

SECTION S – S

TWO PIECES REQUIRED

BREAK ALL SHARP EDGES.

MATERIAL: ALCONITE

PART –03

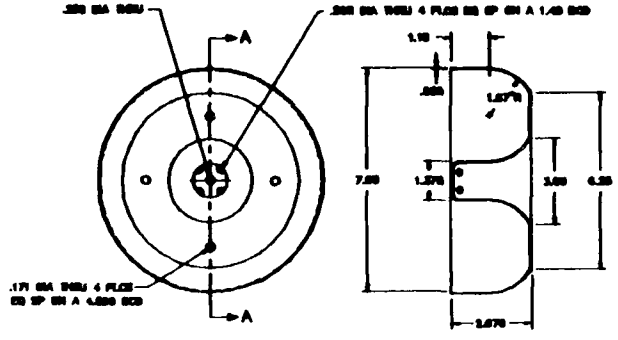

SECTION A – A

TWO PIECES REQUIRED

MATERIAL: 6061 O ALUMINUM

BREAK ALL SHARP EDGES.
SURFACE FINISH TO 32 RMS.

PART –02

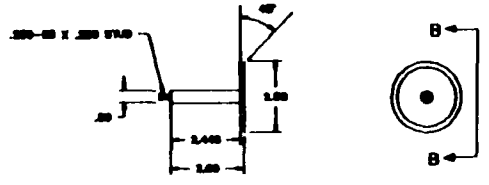

BREAK ALL SHARP EDGES.
SURFACE FINISH TO 32 RMS.

VIEW B – B

PART –04

MATERIAL: 6061 O ALUMINUM

MOD.SWITCH PARTS	
REVISION	DR. G. ESTEPP
Tolerance unless noted	DRAWN BY GNE
.XXXX +/-.005	CHECKED
.XXX +/-.015	DATE 2/10/88
Angles +/-1°	SHEET 1 OF 1
APPROVED	MRC-89709
SCALE FULL	

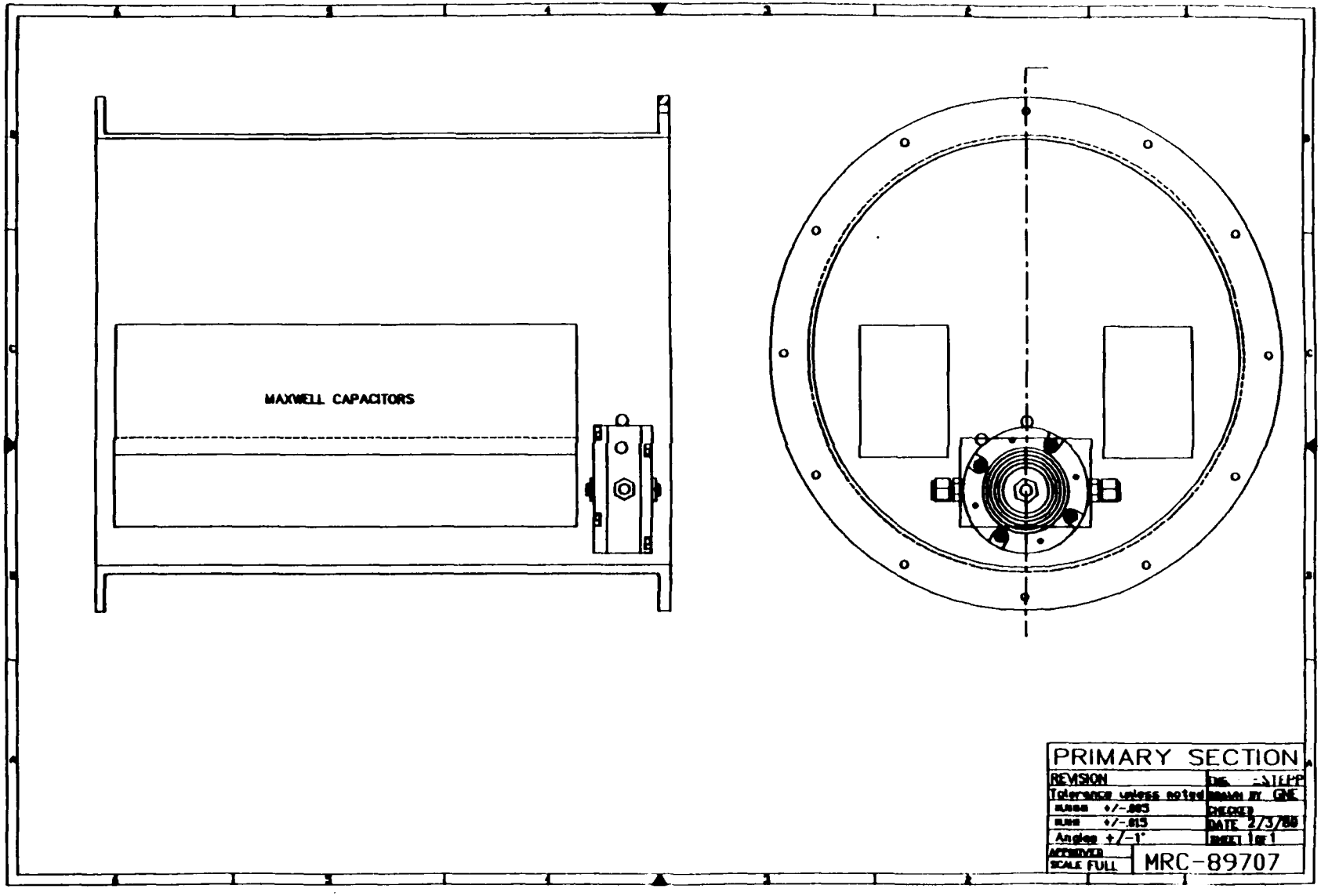
MAXWELL CAPACITORS
PRIMARY SECTION
REVISION
Tolerance unless noted
.xxx +/-.005
.xxx +/-.015
Angles +/-1°
SCALE FULL
DRAWN BY GNE
CHECKED
DATE 2/3/88
SHEET 1 of 1
MRC-89707

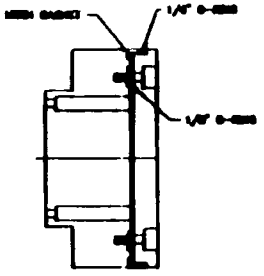

ASSEMBLY

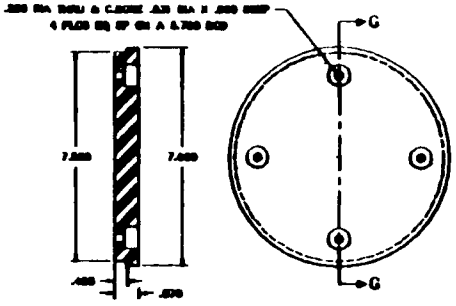

SECTION G – G

MATERIAL: 6061 ALUMINUM
BREAK ALL SHARP EDGES.
SURFACE FINISH TO 64 RMS MINIMUM.

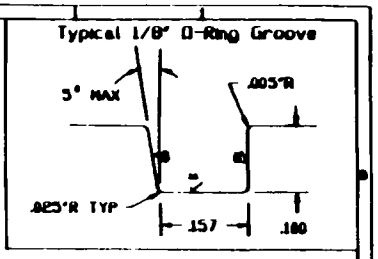

PART –02

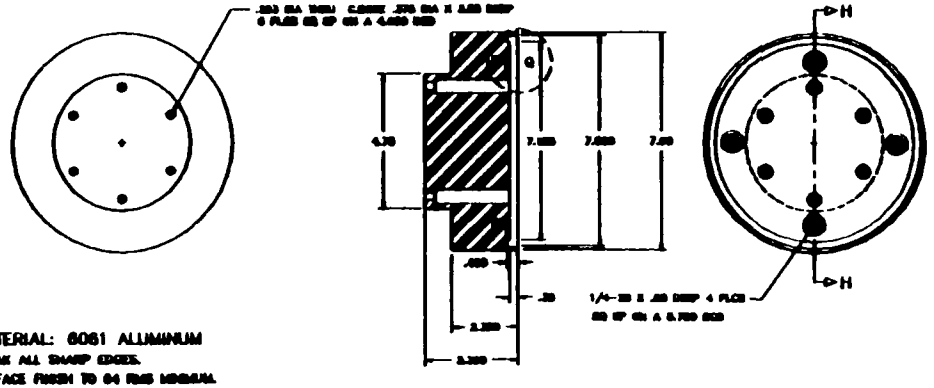

MATERIAL: 6061 ALUMINUM
BREAK ALL SHARP EDGES.
SURFACE FINISH TO 64 RMS MINIMUM.

SECTION H – H

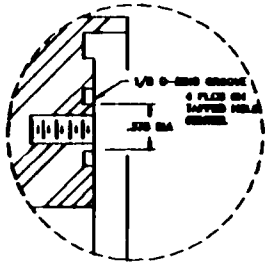

DETAIL Q – Q

PART –01

OUTPUT CONNECTOR	
REVISION	DWG G. ESTEPP
Tolerance unless noted	DRAWN JR CAE
.xxxx +/-.005	CHECKED
.xx +/-.015	DATE 2/2/00
Angles +/-1°	SHEET 1 OF 1
APPROVED	MRC-89708
SCALE FULL	

APPENDIX B
PRIME POWER REQUIREMENTS AFWAL QUICK LOOK REPORT

DEPARTMENT OF THE AIR FORCE
AIR FORCE WRIGHT AERONAUTICAL LABORATORIES (AFSC)
WRIGHT-PATTERSON AIR FORCE BASE, OHIO 45433-6563

REPLY TO ATTN OF: AFWAL/POOS-2 (R. A. Marsh, AV785-7770)

3 APR 1987

SUBJECT: Prime Power Requirements - Quick Look

TO: AD/XRX (Maj V. P. Befi)
Eglin AFB, FL 32542-5000

1. Reference is made to your 11 March 1987 letter, same subject, requesting battery and power supply data.

2. Our examination of six (6) different battery power supplies against your requirements is summarized in the attached memo.

3. For further information regarding batteries, contact R. A. Marsh/ AFWAL/POOS-2/AV 785-7770 or power conditioning contact L. D. Massie/ AFWAL/POOC-1/AV 785-5179.

William A. Seward

WILLIAM A. SEWARD, Major, USAF
Deputy Director
Aerospace Power Division
Aero Propulsion Laboratory

1 Atch
Memo for the Record

Don,

Here is the Prime Power package I was referring to.

Vinny

L SC

87106

Memo For The Record 3 April 1987

Subject: Prime Power Requirements - Quick Look

To: AD/XRX (Maj V. P. Befi)

Rechargeable and non-rechargeable batteries were examined against the requirements stated in the AD/XRX letter dated 11 March 1987.

The rechargeable batteries examined were: Nickel-Cadmium (Ni-Cd), Nickel-Zinc (Ni-Zn) and Silver Oxide-Zinc (AgO-Zn). Ni-Cd batteries provide the longest service and cycle life (300 cycles and 10-15 years service) the Ni-Zn batteries are intermediate (50 cycles and 5-10 years service) and the AgO-Zn batteries provide 10 to 20 cycles over a two year service life. If a rechargeable battery system is used, battery charging is required prior to the mission. The rechargeable battery data is for off-the-shelf, conventional designs. Improved rechargeable batteries are under development and will be available in the mid 1990's. These improved rechargeable batteries will provide significant weight and volume reductions and increased cycle-life capability.

The non-rechargeable batteries examined were reserve batteries which require activation prior to use. The activation process is automatic after a signal, small electric pulse, has been provided. The specific non-rechargeable batteries examined were lithium aluminum-iron disulfide thermal ($LiAl-FeS_2$), lithium-thionyl chloride ($Li-SOCl_2$) and lithium-chlorine thermal ($Li-Cl_2$). The $LiAl-FeS_2$ thermal batteries are widely used in tactical systems and have munitions type storability (15-20 years), operation over a wide temperature range (-65°F to +165°F) and are rugged, one-shot devices. The $Li-SOCl_2$ liquid reserve battery has been in development for the past ten years and is now beginning to find use in weapon systems. The $Li-SOCl_2$ battery low temperature performance is marginal below -20°F and storage life is around 5-10 years. The $Li-Cl_2$ thermal battery is in exploratory development and should be available in the early 1990's.

The power conditioning equipment, to boost the voltage, is 92% efficient (see Appendix A). The battery output power was calculated by dividing the weapon power requirement by 0.92. The four weapon power requirements examined were: 3 kw at 70 kv for ten minutes; 30 kw at 70 kv for ten minutes; 60 kw at 70 kv for ten minutes; 1 milliamp at 15kv for ten minutes. The results of our examination of the various battery types and power requirements are tabulated in Appendix B.

Wayne S. Bishop

WAYNE S. BISHOP
TAM, Batteries and Fuel Cells
Power Technology Branch
Aerospace Power Division
Aero Propulsion Laboratory

POWER PROGRAM FOR EDWARDS AFB [redacted] APPLICATION

- AFWAL/POOC INPUT -

25 MARCH 1987

L.D. Massie
AFWAL/POOC-1
Ext. 55179

POWER CONDITIONING PROBLEM FOR EGLIN AFB HPM APPLICATION

- AFWAL/POOC -

A. Problem Nr. 1: Provide estimates of the size and weight of Power Conditioning for the following cases:

1. 3 Kilowatts (Average), 70 Kilovolts, 10 Minutes, Battery Source at 500 Volts Input.

2. 30 Kilowatts (Average), 70 Kilovolts, 10 Minutes, Battery Source at 500 Volts Input.

3. 60 Kilowatts (Average), 70 Kilovolts, 10 Minutes, Battery Source at 500 Volts Input.

****

ASSUMPTIONS:

- At 3 Kilowatts (Average):

  P.C. = 92 Percent Efficiency, 6 Watts/Cubic Inch and 3.0 Kilograms/Kilowatt

- At 30 Kilowatts (Average):

  P.C. = 92 Percent Efficiency, 30 Watts/Cubic Inch and .75 Kilograms/Kilowatt

- At 60 Kilowatts (Average):

  P.C. = 92 Percent Efficiency, 30 Watts/Cubic Inch and .75 Kilograms/Kilowatt

****

	WEIGHT (Kg)	VOLUME (Cubic Inches)
At 3 Kilowatts	9	512
At 30 Kilowatts	22.5	1000
At 60 Kilowatts	45	2000

F. Problem Nr. 2: Provide estimates of the size and weight of Power Conditioning for the following case:

1. 15 Kilovolts, 1 Milliampere, 10 Minutes, From Battery Source at 500 Volts Input.

****

ASSUMPTIONS: o P.C. = 92 Percent Efficiency, 200 Kilograms/Kilowatt (High due to Large Fixed Weight) and .10 Watts/Cubic Inch (Low due to Large Fixed Weight)

****

P.C. Weight = .015 Kilowatts X 200 Kilograms/Kilowatt = 3.0 Kilograms

P.C. Size = 15 Watts/.10 Watts/Cubic Inch = 150 Cubic Inches

APPENDIX B. BATTERY/POWER CONDITIONING/SYSTEM PROPERTIES

MISSION	BATTERY					POWER CONDITIONING		POWER SYSTEM	
	CHEMISTRY	TYPE	VOLTAGE (volts)	WT (lbs)	VOLUME (cu in)	WT (lbs)	VOLUME (cu in)	WT (lbs)	VOLUME (cu in)
1. 3kW, 70KV 10 min	LiAl-FeS2	P	50	47	214	19.8	512	66.8	726
	Li-SOCl2	P	100	17.5	207			37.3	719
	Li-Cl2	P	100	6.8	109			26.6	621
	Ni-Cd	R	100	137	2066			156.8	2578
	Ni-Zn	R	100	40	572			59.8	1084
	AgO-Zn	R	100	23	383			42.8	895
2. 30kw,70KV 10 min	LiAl-FeS2	P	100	266	3450	49.5	1000	315.5	4450
	Li-SOCl2	P	100	145	1740			194.5	2740
	Li-Cl2	P	100	55	906			104.5	1906
	Ni-Cd	R	100	580	5665			629.5	6665
	Ni-Zn	R	100	273	4063			322.5	5063
	AgO-Zn	R	100	258	3638			305.5	4688
3. 60Kw,70KV 10 min	LiAl-FeS2	P	150	506	8742	99	2000	605	10742
	Li-SOCl2	P	100	288	3300			387	5300
	Li-Cl2	P	100	109	1670			208	3670
	Ni-Cd	R	100	1160	11300			1259	13300
	Ni-Zn	R	100	550	8200			649	10200
	AgO-Zn	R	100	300	4200			399	6200
4. 15KV, 1ma 10 min	LiAl-FeS2	P	28	2.3	11	6.6	150	8.9	161
	Li-SOCl2	P	75	0.22	2.5			6.82	152.5
	Ni-Cd	R	20	0.50	8			7.1	158
	Ni-Zn	R	20	0.35	5.5			6.95	155.5
	AgO-Zn	R	20	0.25	4.4			6.85	154.4

P= PRIMARY
R= RECHARGEABLE

NOTE: THE RECHARGEABLE BATTERY DATA WAS ESTABLISHED USING "OFF THE SHELF", EXISTING CELL SIZES THAT ARE LISTED IN MANUFACTURER'S CATALOGS AND ARE AVAILABLE WITHOUT DEVELOPMENT.